

Accepted Manuscript

Neurogenic and neuroprotective donepezil-flavonoid hybrids with sigma-1 affinity and inhibition of key enzymes in Alzheimer's disease

Martín Estrada Valencia, Clara Herrera-Arozamena, Lucía de Andrés, Concepción Pérez, José A. Morales-García, Ana Pérez-Castillo, Eva Ramos, Alejandro Romero, Dolores Viña, Matilde Yáñez, Erik Laurini, Sabrina Pricl, María Isabel Rodríguez-Franco



PII: S0223-5234(18)30582-8

DOI: [10.1016/j.ejmech.2018.07.026](https://doi.org/10.1016/j.ejmech.2018.07.026)

Reference: EJMECH 10561

To appear in: *European Journal of Medicinal Chemistry*

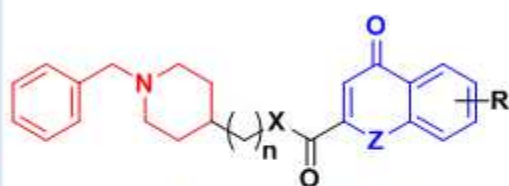
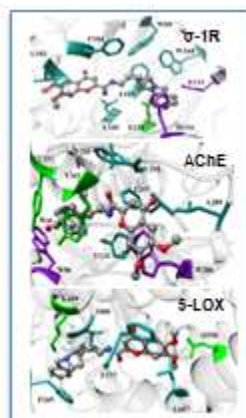
Received Date: 29 May 2018

Revised Date: 18 June 2018

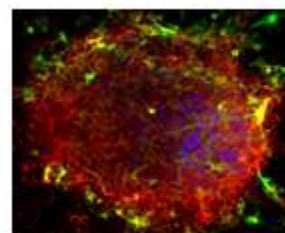
Accepted Date: 9 July 2018

Please cite this article as: Martí. Estrada Valencia, C. Herrera-Arozamena, Lucí. de Andrés, Concepción Pérez, José.A. Morales-García, A. Pérez-Castillo, E. Ramos, A. Romero, D. Viña, M. Yáñez, E. Laurini, S. Pricl, Mari.Isabel. Rodríguez-Franco, Neurogenic and neuroprotective donepezil-flavonoid hybrids with sigma-1 affinity and inhibition of key enzymes in Alzheimer's disease, *European Journal of Medicinal Chemistry* (2018), doi: 10.1016/j.ejmech.2018.07.026.

This is a PDF file of an unedited manuscript that has been accepted for publication. As a service to our customers we are providing this early version of the manuscript. The manuscript will undergo copyediting, typesetting, and review of the resulting proof before it is published in its final form. Please note that during the production process errors may be discovered which could affect the content, and all legal disclaimers that apply to the journal pertain.



- > Sigma-1 receptor, K_i s \approx 1 – 45 nM
- > AChE, IC_{50} s \approx 21 – 100 nM
- > 5-LOX, IC_{50} s \approx 4 – 90 μ M
- > MAO-A/B, IC_{50} s \approx 5 – 70 μ M
- > ROS-trapping capacities
- > CNS-permeable compounds



- > Neuroprotection vs. mitochondrial oxidative stress
- > Maturation of neural stem cells to neuronal phenotype

ACCEPTED MANUSCRIPT

Neurogenic and neuroprotective donepezil-flavonoid hybrids with sigma-1 affinity and inhibition of key enzymes in Alzheimer's disease

Dedicated to the memory of our dear colleague Dr. Elena Soriano

Martín Estrada Valencia^a, Clara Herrera-Arozamena^a, Lucía de Andrés^a, Concepción Pérez^a, José A. Morales-García^{b,c,d}, Ana Pérez-Castillo^{b,c}, Eva Ramos^e, Alejandro Romero^e, Dolores Viña^f, Matilde Yáñez^g, Erik Laurini^h, Sabrina Prici^h, and María Isabel Rodríguez-Franco^{a,*}

^aInstituto de Química Médica, Consejo Superior de Investigaciones Científicas (IQM-CSIC), C/ Juan de la Cierva 3, 28006-Madrid, Spain.

^bInstituto de Investigaciones Biomédicas “Alberto Sols”, Consejo Superior de Investigaciones Científicas (IIB-CSIC), C/Arturo Duperier 4, 28029-Madrid, Spain.

^cCentro de Investigación Biomédica en Red sobre Enfermedades Neurodegenerativas (CIBERNED), C/ Valderrebollo 5, 28031-Madrid, Spain.

^dDepartamento de Biología Celular, Facultad de Medicina, Universidad Complutense de Madrid, 28040-Madrid, Spain.

^eDepartamento de Farmacología y Toxicología, Facultad de Veterinaria, Universidad Complutense de Madrid, 28040-Madrid, Spain.

^fCenter for Research in Molecular Medicine and Chronic Diseases (CIMUS), Universidad de Santiago de Compostela, 15782-Santiago de Compostela, Spain.

^gDepartamento de Farmacología, Facultad de Farmacia, Universidad de Santiago de Compostela, 15782-Santiago de Compostela, Spain.

^hMolecular Simulation Engineering (MOSE) Laboratory, Department of Engineering and Architecture (DEA), University of Trieste, 34127 Trieste, Italy.

*Corresponding Author

E-mail address: isabelrguez@iqm.csic.es

Keywords:

Donepezil-flavonoid hybrids

Neurogenesis

Neuroprotection

Sigma receptors

Human acetylcholinesterase

Human 5-lipoxygenase

Human monoamine oxidases

Highlights:

- Donepezil-flavonoid hybrids with high affinity for sigma-1 receptors
- Inhibition of acetylcholinesterase, 5-lipoxygenase, and monoamine oxidases
- Many donepezil-flavonoid hybrids are radical-scavenger and brain-permeable
- Neuroprotection vs. mitochondrial oxidative stress in human neuroblastoma
- Hybrid **18** stimulates differentiation of stem-cells to a neuronal phenotype *in vitro*

Abbreviations: AChE, acetylcholinesterase; AD, Alzheimer's disease; ATCh, acetylthiocholine; BBB, blood-brain barrier; BOP, (benzotriazol-1-yl)oxytris(dimethylamino)phosphonium hexafluorophosphate; BuChE, butyrylcholinesterase; CAS, catalytic anionic site of AChE; DCM, dichloromethane; DMF, dimethylformamide; CDI, 1,1'-carbonyldiimidazole; CNS, central nervous system; DAPI, 4',6-diamidino-2-phenylindole; DFHs, donepezil - flavonoid hybrids; DTG, 1,3-di-o-tolylguanidine; HMBC, heteronuclear multiple bond correlation; HPLC, high-performance liquid chromatography; HRMS, high resolution mass spectrum; HSQC, heteronuclear single quantum correlation; K_i , binding constant; LB, Lineweaver-Burk method; 5-LOX, 5-lipoxygenase; MAO-A and MAO-B, monoamine oxidase-A and monoamine oxidase-B; MAP-2, microtubule-associated protein 2; MD, Molecular Dynamics; MM/PBSA, Molecular Mechanics/Poisson-Boltzmann Surface Area; MTDLs, multi-target-directed ligands; MTT, 3-[4,5-dimethylthiazol-2-yl]-2,5-diphenyl-tetrazolium bromide; mw, microwave; NDGA, nordihydroguaiaretic acid; NDs, neurodegenerative diseases; NMDA, *N*-methyl-D-aspartate receptor; NMR, nuclear magnetic resonance; NS, neurospheres; NSC, neural stem cells; ORAC, oxygen radical scavenger capacity assay; OS, oxidative stress; PAINS, pan assay interference compound; PAMPA-BBB, parallel artificial membrane permeability assay for the blood-brain barrier; PAS, peripheral anionic site of AChE; P_e , permeability value; PRBFED, per-residue binding free energy deconvolution; PTZ, pentazocine; ROS, radical oxygen species; SEM, standard error of the mean; SGZ, subgranular zone; σ_1R and σ_2R , sigma-1 and sigma-2 receptor; SVZ, subventricular zone; THF, tetrahydrofuran; Tuj1, β -tubulin III marker.

ABSTRACT

In this work we describe neurogenic and neuroprotective donepezil-flavonoid hybrids (DFHs), exhibiting nanomolar affinities for the sigma-1 receptor (σ_1R) and inhibition of key enzymes in Alzheimer's disease (AD), such as acetylcholinesterase (AChE), 5-lipoxygenase (5-LOX), and monoamine oxidases (MAOs). In general, new compounds scavenge free radical species, are predicted to be brain-permeable, and protect neuronal cells against mitochondrial oxidative stress. *N*-(2-(1-Benzylpiperidin-4-yl)ethyl)-6,7-dimethoxy-4-oxo-4*H*-chromene-2-carboxamide (**18**) is highlighted due to its interesting biological profile in σ_1R , AChE, 5-LOX, MAO-A and MAO-B. In phenotypic assays, it protects a neuronal cell line against mitochondrial oxidative stress and promotes maturation of neural stem cells into a neuronal phenotype, which could contribute to the reparation of neuronal tissues. Molecular modelling studies of **18** in AChE, 5-LOX and σ_1R revealed the main interactions with these proteins, which will be further exploited in the optimization of new, more efficient DFHs.

1. Introduction

Alzheimer's disease (AD) is the most common of the age-related neurodegenerative pathologies (NDs), causing devastating health, social, familiar, and economic problems in world-wide countries [1]. AD is characterized by the occurrence of abnormal protein aggregates in the brain (amyloid plaques and neurofibrillary tangles), the loss of synaptic connections, and death of extensive neuronal populations, especially those involved in the intellectual functions [2]. Currently, there are only four drugs in the market for the palliative management of AD: three acetylcholinesterase (AChE) inhibitors (donepezil, rivastigmine, and galantamine) and an antagonist of the *N*-methyl-D-aspartate (NMDA) receptor, i.e., memantine [3].

Due to the highly complex pathophysiology of AD, several combinations of drugs acting at different targets have been probed in clinical trials, such as the mixture of donepezil and memantine that provided superior benefits over monotherapies [4]. In a similar way, the multi-target-directed ligands (MTDLs) paradigm proposes the design of single molecules that were active against several pharmacological targets, in the quest of a superior therapeutic efficacy [5,6]. The MTDL approach would be particularly useful when drugs hit targets involved upstream in neurotoxic cascades, as they could really stop or delay neurodegeneration [7].

Nowadays, the causes that trigger AD are not completely known, but different findings indicate that mitochondrial dysfunctions that increase oxidative stress (OS) and neuroinflammation are at the vertex of many pathological cascades [8]. The implication of OS in AD is supported by different post-mortem studies, which show a considerable increase in the peroxidation of biomolecules (lipids, proteins, and nucleic acids) in the most affected regions of the brain of patients with severe AD [9]. Moreover, it has been proven that cellular oxidative damage is a fact that precedes the appearance of abnormal

protein aggregates [10]. These observations suggest that protective agents against mitochondrial oxidative stress may be useful in the prevention and treatment of AD [11].

On the other hand, several epidemiological studies have revealed that patients under chronic treatment with non-steroidal anti-inflammatory drugs showed a reduction in the risk of developing AD, although the protection mechanism is still a subject of debate [12]. 5-Lipoxygenase (5-LOX), a key enzyme involved in the inflammatory responses, is expressed at higher levels in the hippocampus of patients affected by AD [13]. Contextually, overexpression of 5-LOX leads to memory deficiencies and increase of protein aggregates in transgenic mice [14].

5-LOX catalyses two early steps of the peroxidation of arachidonic acid to leukotriene A₄, which is further transformed to eicosanoids by several enzymatic systems. In the central nervous system (CNS), eicosanoids perform numerous functions of cellular communication, but they are also involved in the activation of inflammatory cascades. Particularly, it has been shown that pro-inflammatory eicosanoids, including leukotriene A₄, increase the expression of amyloid precursor protein (APP), with the consequent growth of pathogenic amyloid plaques [15]. For this reason, inhibitors of 5-LOX have been proposed as potential drugs for the treatment of different diseases, including AD [16].

Monoamine oxidases (MAO-A and MAO-B) are metabolic enzymes that are located on the outer mitochondrial membrane. As for 5-LOX, the brain levels of these proteins are increased in neurodegenerative pathologies, such as AD and Parkinson's disease [17]. Abnormally high concentrations of MAOs enhance the expression of β - and γ -secretases, promoting the formation of the pathogenic β -amyloid peptide from the amyloid precursor protein, and increase the OS by the production of hydrogen peroxide

[18]. Thus, MAOs inhibition could bring beneficial effects in neurotransmission by lowering catabolism of several monoamine neurotransmitters and by reducing the generation of amyloid plaques and radical oxygen species (ROS) [19,20].

Sigma receptors, and in particular the subtype-1 (σ_1 R), are expressed in CNS areas related to emotional and cognitive functions, such as hippocampus and neocortex [21]. Activation of σ_1 R evokes neuroprotection by increasing levels of endogenous antioxidant proteins [22] and by maintenance of mitochondrial respiration and ATP synthesis [23], among other mechanisms. Thus, σ_1 R agonists are potential drugs for AD, such as anavex2-73 that is currently in phase 2a of clinical trials in patients with mild to moderate AD [24].

Although questioned for decades, adult neurogenesis is now recognized as an important mechanism of neuron self-renewal along the life of the individual [25]. In the adult human brain, there are two niches of stem-cells located in the subventricular and the subgranular zones (SVZ and SGZ, respectively), which are capable of generating new neurons [26]. As the neuronal self-repair mechanisms decrease with aging and dramatically fall in NDs and other mental pathologies, the pharmacological stimulation of neurogenic niches might counteract the neuronal loss observed in such diseases [27].

Many signalling pathways involved in neurogenic processes have been identified and different drug types have been recently tested in neuronal plasticity. For instance, antioxidants and σ_1 R agonists have positive effects in the generation and maturation of new neurons from stem-cell niches and also promote new neuronal connections by stimulating neurite outgrowth [28,29].

Therefore, neurogenesis and neuroprotection have recently emerged as innovative and complementary strategies for battling AD [27]. The development of new active

agents capable of protecting the more vulnerable neuronal populations or even replacing damaged neurons with new functionally competent cells, could provide disease-modifying therapeutic regimens for AD [30]. In recent years, our group has reported the synthesis and biological evaluation of several families of MTDLs of potential interest for the treatment of AD, endowed with neuroprotective [31,32] or neurogenic properties [33-36], or even with the combination of both actions [37,38].

Along the latter line of dual activity, in the present effort we developed 29 new donepezil – flavonoid hybrids (DFHs). On one hand, we selected the *N*-benzylpiperidine fragment from donepezil, due to its well-known σ_1 R-agonism and AChE-inhibition [39]. On the other hand, we selected the 4-oxo-4*H*-chromene scaffold present in numerous flavonoids (e.g. apigenin and luteolin), which showed inhibition of MAO [40] and 5-LOX [41,42], as well as antioxidant, anti-inflammatory and neurogenic properties [43]. Indeed, the *C*-glycoside flavonoid spinosin was found to enhance adult hippocampal neurogenesis in mice, linked to an improvement in cognitive performance [44] (Figure 1).

In these new DFHs, the *N*-benzylpiperidine fragment was unchanged due to its well-known excellent fit in the catalytic anionic site of AChE (CAS) [45]. In relation to the potential modifications in the flavonoid scaffold we planned to: (i) change the 4-oxo-4*H*-chromene skeleton by related heterocycles, such as quinolin-4(1*H*)-one or quinoline rings; (ii) introduce methoxy groups to improve interactions with the peripheral anionic site of hAChE (PAS), as previously described [46]; (iii) insert hydroxyl groups to achieve radical capture capacity and 5-LOX inhibition, as described for phenolic hydroxyl derivatives [47]. Finally, we thought connecting *N*-benzylpiperine and flavonoid fragments by a linker of different nature (amide or ester) and length ($n = 0 - 3$).

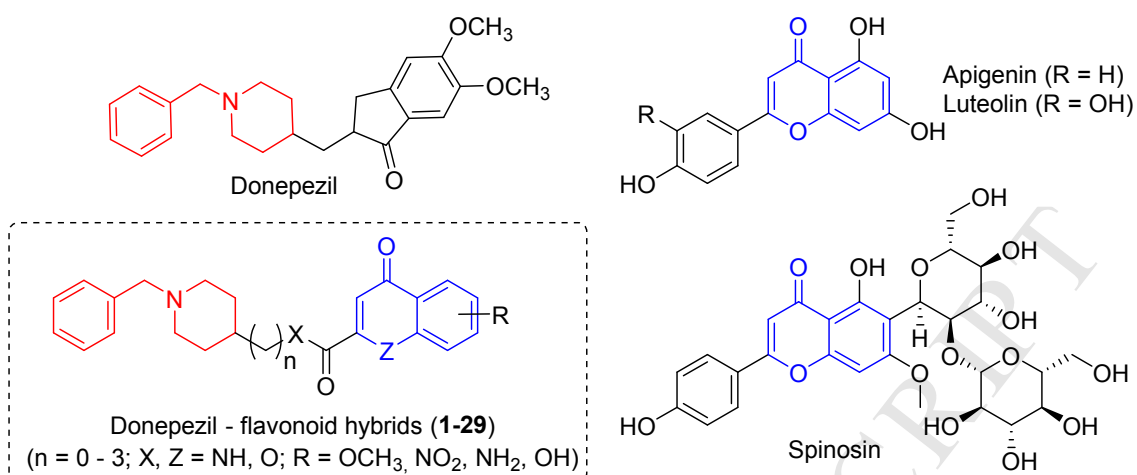


Figure 1. Structures of donepezil, flavonoids (apigenin, luteolin, and spinosin), and donepezil – flavonoid hybrids (DFHs, **1-29**)

Accordingly, in what follows we describe the synthesis of these new DFHs (**1-29**) and their biological evaluation that includes σ_1 R binding, antioxidant properties, *in vitro* CNS penetration, inhibition of 5-LOX, AChE and MAOs, and phenotypic assays of neurogenesis and neuroprotection. Finally, molecular modelling studies have been carried out to elucidate the binding mechanism of DFHs on the three main target proteins, that is AChE, 5-LOX and σ_1 R.

2. Results and discussion

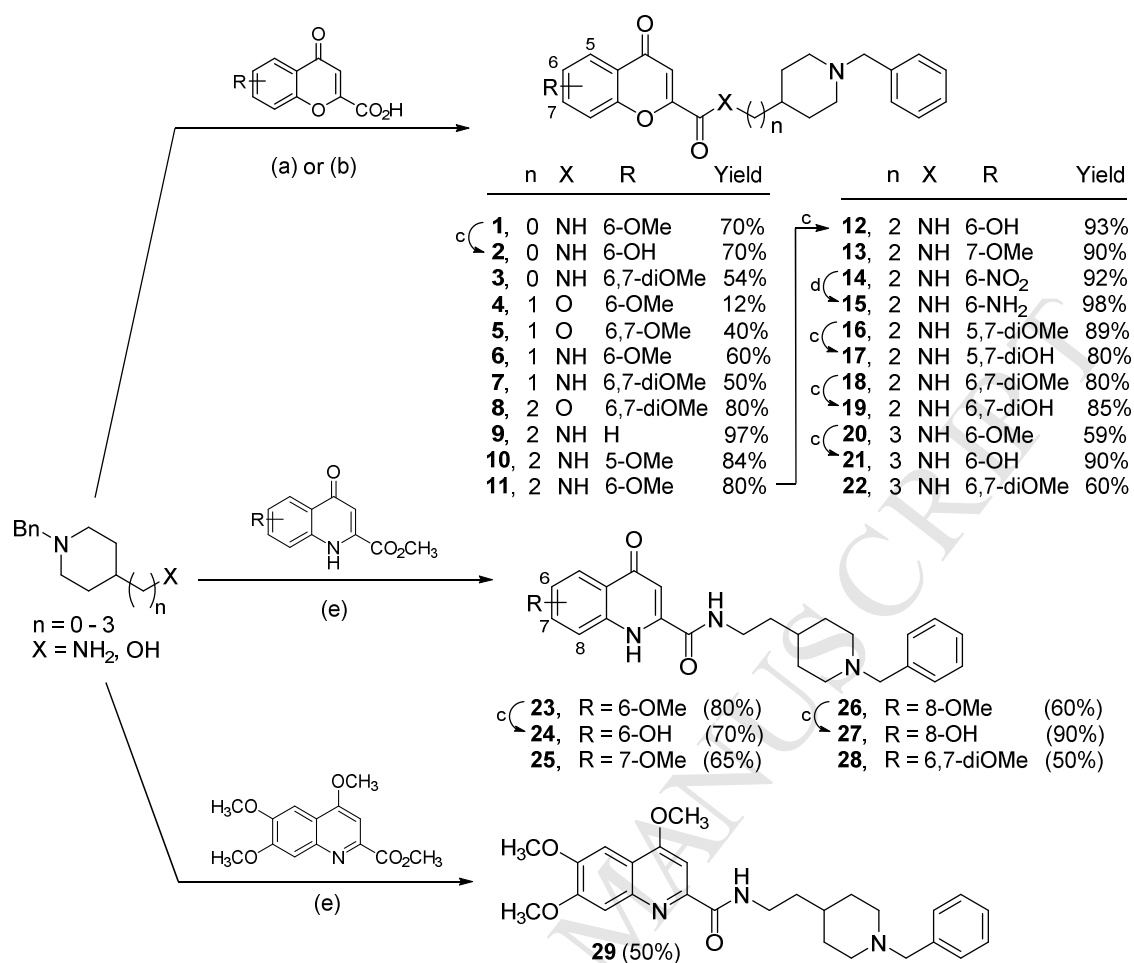
2.1. Synthesis of DFHs

Scheme 1 depicts the synthetic routes for the synthesis of the new hybrids (**1-29**). Some amine and alcohol intermediates derived from *N*-benzylpiperidine are commercially available and others were obtained following previously reported methods [35,38]. 4-Oxo-4*H*-chromene-2-carboxylic acids and methyl quinoline-2-carboxylates were synthesized according to well-known routes [46,48] (see Supporting Information for further details).

The synthesis of chromone-based hybrids **1**, **3-11**, **13**, **14**, **16**, **18**, **20** and **22** was developed by a coupling reaction between the corresponding *N*-benzylpiperidine alcohol or amine and different 4-oxo-4*H*-chromene-2-carboxylic acids, using two different methods: i) a microwave (mw)-assisted reaction with 1,1'-carbonyldiimidazole (CDI) as activating agent, and ii) a coupling reaction at room temperature (rt) with (benzotriazol-1-yloxy)tris(dimethylamino)phosphonium hexafluorophosphate (BOP) and triethylamine (Et₃N). In both cases, dimethylformamide (DMF) was selected as solvent due to the low solubility of the 4-chromone carboxylic acids in less polar solvents. However, when activation is carried out with BOP, other solvents could be used, i.e. tetrahydrofuran (THF) or dichloromethane (DCM), because the Et₃N concurs in acids solubilisation. Hydroxy-chromone hybrids **2**, **12**, **17**, **19** and **21** were obtained via deprotection of the corresponding methoxylated derivative by overnight treatment with boron tribromide (BBr₃) at rt. It is worth-mentioning that, to ensure good reaction yields (70-90%), 1 equivalent of BBr₃ for each ether group to be cleaved, plus an additional 1 equivalent for each heteroatom present in the molecule, must be used [49]. The amino-chromone hybrid **15** was obtained with an almost quantitative yield (98%) by the catalytic hydrogenation of the corresponding nitro derivative **14**.

The 4-quinolone-based hybrids bearing methoxy groups **23**, **25**, **26**, and **28** and the trimethoxyquinoline **29** were obtained by trimethylaluminium [Al(CH₃)₃]-mediated amide formation between the corresponding 4-oxo-1,4-dihydroquinoline or quinoline methyl ester and 2-(1-benzylpiperidin-4-yl)ethan-1-amine (Scheme 1). The use of mw irradiation at 120 °C allowed obtaining the desired products in 1.5 min with medium to good yields (50-90%). Finally, hydroxy-substituted compounds **24** and **27** were obtained by treatment of methoxy derivatives with BBr₃ in THF at rt as previously mentioned.

All DFHs **1-29** were purified in silica gel cartridges using an automatic chromatographic equip (IsoleraPrime, Biotage) and were characterized by their analytical (HPLC, HRMS) and spectroscopic data (¹H NMR, ¹³C NMR). Complete NMR assignment of their hydrogen and carbon atoms were made by ¹H – ¹³C two-dimensional diagrams, mainly HSQC (heteronuclear single quantum correlation) and HMBC (heteronuclear multiple bond correlation). In the case of the 6-nitrochromone hybrid **14** the CH group at position 3 of the 4-chromone system was not observed either in ¹³C or ¹H NMR spectra, although its exact mass by high resolution mass spectroscopy matched the one of the desired product. Moreover, the amino derivative **15**, obtained by hydrogenation of **14**, exhibited all the expected signals and exact mass, allowing us to confirm the structure of the nitro derivative.

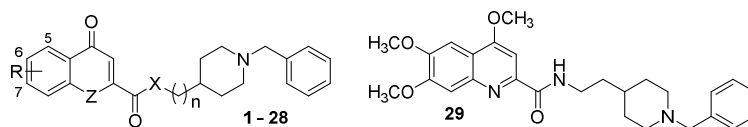


Scheme 1. Reagents and conditions: (a) i) Acid, CDI, DMF, mw, 120 °C, 10 min, ii) amine, mw, 150 °C, 10 min; (b) BOP, Et₃N, DMF, overnight, rt; (c) BBr₃, DCM, overnight, 0 °C → rt; (d) H₂/Pd-C (5%), EtOH, overnight, rt; (e) Al(CH₃)₃, THF, mw, 120 °C, 90 sec.

Unlike the 4-chromone scaffold, the 4-oxo-1,4-dihydroquinoline structure can exist in two tautomeric forms. In the keto tautomer, the hydrogen at position 3 possesses lower aromatic character and consequently, lower chemical shifts should be observed compared with the enol form. Given the lower chemical shifts observed in hybrids **23-28** compared to the full aromatic derivative **29**, we inferred that the keto form is the favoured tautomer in **23-28**. Probably due to this tautomeric equilibrium, some quaternary carbons in the 4-quinolone scaffold were not detected and the multiplicity of some aromatic protons was not well defined, appearing as broad signals. However, high resolution mass spectroscopy confirmed the exact mass of the desired products.

2.2. Inhibition of human cholinesterases, study of inhibitory mechanisms, and prediction of CNS permeation

All new DFHs **1-29** were evaluated as inhibitors of human cholinesterases (hAChE and hBuChE). Following this initial screening, a selection of the most potent inhibitors was studied in Lineweaver-Burk experiments to determine their inhibition mechanisms. Next, in order to establish their ability to reach the CNS all derivatives were also evaluated in the *in vitro* parallel artificial membrane permeability assay for the blood-brain barrier (PAMPA-BBB). All results are gathered in Table 1.

Table 1. Inhibition of human cholinesterases (IC_{50} , nM) and prediction of the CNS-permeation by DFHs (**1-29**).^a

Compd	n	X	Z	R	hAChE IC_{50} (nM)	hBuChE IC_{50} (nM)	hAChE selectivity ^b	PAMPA-BBB P_e (10^{-6} cm s ⁻¹)	CNS prediction
1	0	NH	O	6-OMe	970 ± 40	>10000	>10	7.7 ± 0.7	cns +
2	0	NH	O	6-OH	2360 ± 140	>10000	>4.2	1.9 ± 0.6	cns -
3	0	NH	O	6,7-diOMe	660 ± 50	>10000	>15	8.1 ± 0.3	cns +
4	1	O	O	6-OMe	7490 ± 120	>10000	>1.3	6.1 ± 0.3	cns +
5	1	O	O	6,7-diOMe	300 ± 25	>10000	>33	3.2 ± 0.5	cns +/-
6	1	NH	O	6-OMe	3610 ± 90	>10000	>2.8	6.8 ± 0.3	cns +
7	1	NH	O	6,7-diOMe	1460 ± 70	>10000	>6.8	n.d.	
8	2	O	O	6,7-diOMe	56 ± 5	>10000	>179	5.6 ± 0.3	cns +
9	2	NH	O	H	110 ± 10	5090 ± 360	46	6.7 ± 0.5	cns +
10	2	NH	O	5-OMe	870 ± 14	>10000	>12	n.d.	
11	2	NH	O	6-OMe	170 ± 10	6500 ± 500	38	10.0 ± 0.2	cns +
12	2	NH	O	6-OH	91 ± 8	>10000	>110	2.8 ± 0.4	cns +/-
13	2	NH	O	7-OMe	33 ± 2	9900 ± 900	300	7.6 ± 0.7	cns +
14	2	NH	O	6-NO ₂	21 ± 2	9300 ± 700	443	8.2 ± 0.1	cns +
15	2	NH	O	6-NH ₂	41 ± 3	4300 ± 350	105	7.6 ± 0.2	cns +
16	2	NH	O	5,7-diOMe	320 ± 20	6300 ± 450	20	8.8 ± 0.5	cns +
17	2	NH	O	5,7-diOH	580 ± 40	>10000	>17	3.7 ± 0.5	cns +/-
18	2	NH	O	6,7-diOMe	46 ± 4	>10000	>217	5.9 ± 0.8	cns +
19	2	NH	O	6,7-diOH	4130 ± 190	>10000	>2.4	3.2 ± 0.3	cns +/-
20	3	NH	O	6-OMe	370 ± 13	5800 ± 450	16	10.6 ± 0.1	cns +
21	3	NH	O	6-OH	23 ± 2	>10000	>435	4.5 ± 0.3	cns +
22	3	NH	O	6,7-diOMe	110 ± 10	>10000	>91	5.0 ± 0.3	cns +
23	2	NH	NH	6-OMe	880 ± 40	>10000	>11	12.0 ± 0.5	cns +
24	2	NH	NH	6-OH	300 ± 20	9880 ± 770	33	5.1 ± 0.4	cns +
25	2	NH	NH	7-OMe	450 ± 40	>10000	>22	10.9 ± 0.6	cns +
26	2	NH	NH	8-OMe	1640 ± 70	>10000	>6.1	15.3 ± 1.5	cns +
27	2	NH	NH	8-OH	1150 ± 90	>10000	>8.7	4.9 ± 0.1	cns +
28	2	NH	NH	6,7-diOMe	170 ± 10	>10000	>59	5.3 ± 0.4	cns +
29	2	NH	NH	4,6,7-triOMe	620 ± 50	8790 ± 500	14	13.0 ± 0.8	cns +
Donepezil					10 ± 1	2500 ± 70	250	n.d.	

^aResults are given as mean ± SEM of three independent experiments. ^bSelectivity index for hAChE was calculated as IC_{50} (hBuChE) / IC_{50} (hAChE). n.d., not determined.

Inhibition of hAChE and hBuChE were performed following the Ellman method [50], using donepezil as reference drug. Both series of DFHs, derived either from 4-chromone or 4-quinolone, were found to be selective inhibitors of hAChE with IC_{50} values from the low micromolar to the nanomolar range, in some cases very close to the donepezil IC_{50} value (10 nM). Inhibition of hBuChE was substantially less effective, with IC_{50} above 10 μ M for the majority of new compounds (Table 1). As a result, many hybrids showed a high preference for hAChE with selectivity indexes comparable to or even exceeding the one of donepezil, which currently is the most used drug in the treatment of AD.

By comparing the two classes of DFHs, 4-chromone-derived compounds (**11-13** and **18**, with IC_{50} s = 33-170 nM) were more potent hAChE inhibitors than their 4-quinolone counterparts (**23-25** and **28**, with IC_{50} s = 170-880 nM). This fact highlights the relevance of the endocyclic oxygen and/or the stability of the exocyclic carbonyl group in the 4-chromenone ring in the interaction with the enzyme, since its substitution with a heterocycle susceptible of tautomerization (4-quinolinone) was detrimental to activity.

In general, 4-chromone-based hybrids with an aliphatic linker of 2 or 3 methylene groups were more potent and selective hAChE inhibitors than their counterparts with shorter linkers ($n = 0$ or 1). Replacement of an amide by an ester bond did not affect significantly the inhibitory potency, as evidenced by comparing IC_{50} values for the ester derivative **8** and its amide counterpart **18** (56 nM and 46 nM, respectively).

Regarding amide derivatives, the nature and position of substituents in the heterocyclic moiety yielded interesting effects on the hAChE inhibition. Best results were obtained when substituents were located at positions 6 and / or 7 of the 4-oxo-4H-chromene ring, whereas position 5 appeared to be detrimental for activity. The most

potent hAChE inhibitors were **14** (6-NO₂), **21** (6-OH), **13** (7-OMe), **15** (6-NH₂), **18** (6,7-diOMe), and **12** (6-OH) with IC₅₀ values comprised between 21 and 91 nM.

A set of potent hAChE inhibitors including further different structural features (**8**, **9**, **14**, **15**, **18**, **21**, **22**, and **28**) were selected for studying reaction kinetics between the enzyme and these 4-chromone- or 4-quinolone-based hybrids. Following the Lineweaver-Burk (LB) method, the initial velocity of enzymatic inhibition was measured at four concentrations of the substrate acetylthiocholine (ATCh), in absence and presence of increasing concentrations of the inhibitor. For each inhibitor concentration, the plot of the reciprocals of both velocity and ATCh concentration ($1/V$ vs. $1/[ATCh]$) gave straight lines that were fitted by least-squares analysis, allowing the determination of the corresponding kinetic parameters (i.e., the Michaelis constant K_m and the maximum velocity V_{max}). For all DFH molecules studied, both $1/V_{max}$ (y intercept) and $-1/K_m$ (x intercept) increased with increasing inhibitor concentration. Figure 2 shows the LB analysis for the 4-chromone – *N*-benzylpiperidine hybrid **18** as an example (see Supporting Information for the full set of LB graphs). This common trend let us speculate that both competitive and non-competitive mechanisms are at play in the enzymatic inhibition by the present DFHs, suggesting the simultaneous interaction of the hybrids with two significant sites of hAChE, CAS and PAS. For each tested compound, replot of slopes vs. inhibitor concentration gave a straight line that was also fitted by least-squares analysis and whose intersection on the negative x-axis provided the calculated inhibition constants (K_i) listed in Table 2.

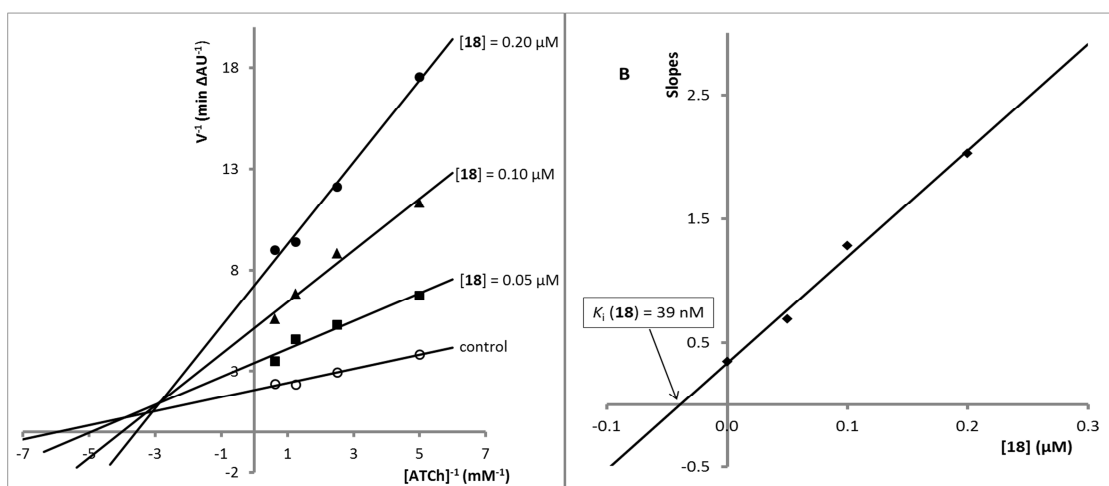


Figure 2. Kinetic study on the mechanism of hAChE inhibition by hybrid **18**. (A) Overlaid Lineweaver-Burk reciprocal plots of hAChE initial velocity at increasing substrate concentration (ATCh, 0.2 – 1.6 mM) in the absence of inhibitor and in the presence of **18** (0 – 0.20 μM) are shown. Lines were derived from a least-squares analysis of the data points. (B) Replot of slopes vs. inhibitor concentration for calculating K_i as the intersection on the x-axis.

Table 2. hAChE inhibition constants (K_i , nM) of selected DFHs^a.

Compd.	n	X	Z	R	K_i (nM)
8	2	O	O	6,7-diOMe	11
9	2	NH	O	H	57
14	2	NH	O	6-NO ₂	12
15	2	NH	O	6-NH ₂	62
18	2	NH	O	6,7-diOMe	39
21	3	NH	O	6-OH	11
22	3	NH	O	6,7-diOMe	21
28	2	NH	NH	6,7-diOMe	60

^aCalculated from LB experiments by replotting slopes vs. inhibitor concentration.

Since a favourable CNS penetration is indispensable for effective drugs against AD and other cerebral pathologies, the *in vitro* evaluation of the capacity of these new molecules to cross the blood-brain barrier (BBB) is of particular interest in early stages of pharmaceutical research. In this work, we used the *in vitro* PAMPA-BBB assay originally described by Di et al. [51], and partially modified by us for testing molecules with limited water-solubility [37,52-54]. Accordingly, the passive CNS-permeation (P_e) of the new DFH compounds through a lipid extract of porcine brain was measured at room temperature, and these results are reported in the last column of Table 1. In the same assay, 11 commercial drugs were also tested for comparison, and their permeability values were normalized to the reported PAMPA-BBB data (see Supporting Information for further details). According to the established literature values [51], compounds with P_e exceeding $4 \cdot 10^{-6} \text{ cm s}^{-1}$ should be able to cross the blood-brain barrier (cns+), whereas those displaying P_e lower than $2 \cdot 10^{-6} \text{ cm s}^{-1}$ will not reach the CNS (cns-). Between these values, CNS permeability is uncertain (cns +/-).

With the exception of some hydroxyl derivatives, which according to their P_e values could experience some difficulties in passing the BBB (i.e., **2**, **12**, **17**, and **19**), the majority of new 4-chromone- and 4-quinolone-based hybrids synthesized in this work were characterized by permeability values greater than $4 \cdot 10^{-6} \text{ cm s}^{-1}$ (Table 1). Thus, according to this *in vitro* BBB model, it is expected all these compounds can penetrate the CNS by passive diffusion and thus, they could interact with their biological targets.

2.3. Inhibition of human 5-lipoxygenase (5-LOX)

The inhibition of human 5-LOX was performed following the fluorescence-based method described by Pufahl et al. [55], using the two well-known inhibitors (*R,S*)-

zileuton and nordihydroguaiaretic acid (NDGA) as reference drugs. From the results shown in Table 3, some structure – activity relationships could be deduced. In general, 4-chromone-based hybrids resulted to be better inhibitors than the 4-quinolone derivatives, reaching IC_{50} values between one- and two-digit micromolar ranges. The most active 5-LOX inhibitors were **19** ($n = 2$, $R = 6,7\text{-diOH}$), **14** ($n = 2$, $R = 6\text{-NO}_2$), and **21** ($n = 3$, $R = 6\text{-OH}$) with IC_{50} values comprised between 4.2 and 15.1 μM .

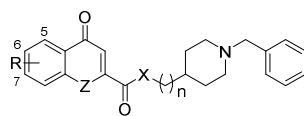
The nature of the substituents in the 4-chromone ring was reflected in major differences in the 5-LOX inhibition, leading to the following potency rank: hydroxyl > nitro > amino > methoxy groups. The amount and position of substituents in the heterocycle also exerted some influences on the activity of the relevant compounds. In general, dihydroxyl compounds were endowed with higher inhibitory potency than chromones bearing one hydroxyl group. Moreover 6,7-positions were preferred over other positions for activity. These observations are evident when comparing the performance of **19** ($n = 2$, $R = 6,7\text{-diOH}$), which is the best inhibitor of the series ($IC_{50} = 4.2 \mu\text{M}$), with **17** ($n = 2$, $R = 5,7\text{-diOH}$, $IC_{50} = 95.1 \mu\text{M}$) and **12** ($n = 2$, $R = 6\text{-OH}$, $IC_{50} > 100 \mu\text{M}$). Apparently, the linker length (methylene number = 0, 2 or 3) between the 4-chromone moiety and the *N*-benzylpiperidine scaffolds could also influenced 5-LOX inhibition, as 6-hydroxychromone hybrids with 0 or 2 methylene linkers (**2** and **12**, respectively) were inactive, whereas their counterpart with a 3-methylene chain **21** showed a good IC_{50} value (15.1 μM). It is noteworthy that hybrid **18** ($n = 2$, $R = 6,7\text{-diOMe}$) showed a moderate inhibition of 5-LOX ($IC_{50} = 74.3 \mu\text{M}$).

2.4. Human MAOs inhibition and antioxidant properties

The next step in the assessment of the multi-target profile of these new DFH compounds was the evaluation of their ability to inhibit both isoforms of human

recombinant MAO, expressed in baculovirus infected BTI insect cells. (*R*)-Deprenyl, iproniazid, and moclobemide were also tested as reference compounds. All results are summarized in Table 3. Several of the DFHs tested were moderate h-MAO inhibitors with 2-digit micromolar IC_{50} s, i.e., in the same range of values displayed by iproniazid and moclobemide. In both MAO subtypes, the most potent inhibitor of the series was the 6,7-dimethoxy-4-oxo-4*H*-chromene hybrid **18**, which proved to be 3-times more active in inhibiting hMAO-B ($IC_{50} = 5.2 \mu\text{M}$) with respect to hMAO-A ($IC_{50} = 15.3 \mu\text{M}$). Regarding selectivity, the 6-nitro-4-oxo-4*H*-chromene hybrid **14** showed an interesting preference toward hMAO-A (>5-fold), whereas the 8-hydroxy-4-oxo-1*H*-quinoline derivative **27** was about 7-fold more active in hMAO-B than in hMAO-A. It is worth-mentioning that high *in vitro* potencies for the inhibition of MAOs are not required to achieve therapeutic effects *in vivo*. For instance, iproniazid and moclobemide that are currently used in the clinics for the treatment of psychiatric and neurological disorders, are characterized by $IC_{50}(\text{MAO-A}) = 6.67$ and $361 \mu\text{M}$, respectively [56].

The antioxidant activities of newly synthesized DFHs were evaluated using the oxygen radical scavenger capacity assay (ORAC) and trolox as reference compound. Trolox is a water-soluble analogue of vitamin E, which contains the aromatic part responsible for the radical capture capacity of this vitamin. Results were expressed as trolox equivalents (μmol of trolox / μmol of tested compound) in a comparative scale where $\text{ORAC}(\text{trolox}) = 1.0$ (Table 3, last column). As expected, compounds bearing methoxy or nitro groups in the heterocyclic scaffold were inactive, while hybrids with amine or hydroxyl groups exhibited interesting antioxidant capacities, ranging from 0.9 to 1.7-fold the trolox value.

Table 3. Inhibition of human 5-LOX and MAOs (IC₅₀, μM); oxygen radical absorbance capacity (ORAC, trolox equiv.)^a

Compd.	n	X	Z	R	5-LOX (IC ₅₀ , μM)	MAO-A (IC ₅₀ , μM)	MAO-B (IC ₅₀ , μM)	ORAC (trolox equiv.)
2	0	NH	O	6-OH	>100 (48%) ^b	n.d.	n.d.	n.d.
7	1	NH	O	6,7-diOMe	>100 (45%) ^b	n.d.	n.d.	n.d.
9	2	NH	O	H	>100 (24%) ^b	n.d.	n.d.	n.d.
11	2	NH	O	6-OMe	>100 (33%) ^b	> 100	> 100	n.d.
12	2	NH	O	6-OH	>100 (36%) ^b	39.3 ± 2.8	51.2 ± 4.3	1.2 ± 0.1
13	2	NH	O	7-OMe	>100 (31%) ^b	> 100	> 100	n.d.
14	2	NH	O	6-NO ₂	9.8 ± 0.7	20.5 ± 1.3	> 100	n.a.
15	2	NH	O	6-NH ₂	28.9 ± 2.5	> 100	> 100	0.9 ± 0.1
17	2	NH	O	5,7-diOH	95.1 ± 4.1	n.d.	n.d.	0.8 ± 0.1
18	2	NH	O	6,7-diOMe	74.3 ± 3.2	15.3 ± 1.3	5.2 ± 0.3	n.a.
19	2	NH	O	6,7-diOH	4.2 ± 0.9	70.5 ± 8.6	37.9 ± 4.2	1.7 ± 0.2
20	3	NH	O	6-OMe	82.4 ± 3.2	> 100	> 100	n.a.
21	3	NH	O	6-OH	15.1 ± 2.9	> 100	> 100	1.3 ± 0.1
22	3	NH	O	6,7-diOMe	>100 (48%) ^b	> 100	> 100	n.a.
23	2	NH	NH	6-OMe	>100 (31%) ^b	> 100	> 100	n.a.
24	2	NH	NH	6-OH	n.d.	51.3 ± 6.2	59.9 ± 6.7	1.4 ± 0.1
25	2	NH	NH	7-OMe	>100 (31%) ^b	72.7 ± 6.5	56.4 ± 4.5	n.a.
26	2	NH	NH	8-OMe	>100 (47%) ^b	52.4 ± 3.1	71.6 ± 5.4	n.a.
27	2	NH	NH	8-OH	77.6 ± 4.6	> 100	13.6 ± 0.9	1.0 ± 0.1
28	2	NH	NH	6,7-diOMe	>100 (31%) ^b	> 100	> 100	n.a.
(<i>R,S</i>)-Zileuton					0.15 ± 0.03	n.d.	n.d.	n.d.
Nordihydroguaiaretic acid (NDGA)					0.10 ± 0.02	n.d.	n.d.	n.d.
(<i>R</i>)-Deprenyl					n.d.	68.7 ± 4.2	0.017 ± 0.002	n.d.
Iproniazid					n.d.	6.67 ± 0.8	7.5 ± 0.36	n.d.
Moclobemide					n.d.	361.4 ± 19.4	> 1000	n.d.

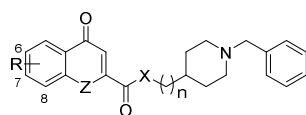
^aResults are given as mean ± SEM from five experiments. ^bIn brackets, inhibition percentage at 100 μM. n.d.: not determined. n.a.: not antioxidant at 10 μM.

2.5. Affinity studies on σ_1 and σ_2 receptors

A selection of 4-chromone and 4-quinolone hybrids displaying different degree of inhibition of human AChE, MAO-A/B, and 5-LOX, and covering also different structural motifs, was investigated for their affinity on sigma receptors of animal origin, obtained from guinea pig brain (σ_1) and rat liver (σ_2), respectively. The affinities of the DFHs for both receptors were determined in competition experiments with the appropriated radioligands. Specifically, [^3H]-(+)-pentazocine (PTZ) served as the radioligand for the σ_1 assay, while [^3H]-1,3-di-o-tolylguanidine (DTG) was employed in the σ_2 assay [57].

All tested compounds showed good affinities for the $\sigma_1\text{R}$, with K_i values between the sub-nanomolar and the two-digit nanomolar range. Affinity values for the $\sigma_2\text{R}$ were in the three-digit nanomolar range, ultimately yielding a σ_1/σ_2 preference of at least 6-times (in the worst case) (Table 4).

The best $\sigma_1\text{R}$ affinity values were provided by compounds bearing a hydrogen-bond acceptor group in the position 6 of the heterocyclic scaffold, which can be ranked as follows: $\text{NO}_2 > \text{NH}_2 > \text{OH} > \text{OCH}_3$. The substitution of the 4-oxo-chromene or 4-oxo-quinoline ring at different positions or the presence of a double substitution led to a decrease of the $\sigma_1\text{R}$ binding capability, although the K_i values remained in the nanomolar range. No significant differences were detected between the 4-oxo-chromene ($Z = \text{O}$) or 4-oxo-quinoline ($Z = \text{NH}$) aromatic moieties. Also, the length of the alkyl spacer between the amide group and the *N*-benzylpiperidine moiety did not seem to affect the $\sigma_1\text{R}$ affinity.

Table 4. Affinity and selectivity of a set of DFHs for σ_1 and σ_2 receptors

Compd.	n	X	Z	R	K_i (nM) ^a		Selectivity for σ_1R ^b
					σ_1R	σ_2R	
12	2	NH	O	6-OH	42.1 ± 9.3	345 ± 78	8
14	2	NH	O	6-NO ₂	0.98 ± 0.32	287 ± 43	293
15	2	NH	O	6-NH ₂	1.45 ± 0.57	421 ± 106	290
18	2	NH	O	6,7-diOMe	37.4 ± 6.3	239 ± 36	6
19	2	NH	O	6,7-diOH	27.0 ± 6.1	278 ± 33	10
21	3	NH	O	6-OH	3.48 ± 1.26	301 ± 59	87
23	2	NH	NH	6-OMe	7.2 ± 2.4	459 ± 83	64
25	2	NH	NH	7-OMe	45.2 ± 10.7	376 ± 64	8
27	2	NH	NH	8-OH	47.4 ± 7.5	290 ± 42	6
28	2	NH	NH	6,7-diOMe	36.3 ± 5.0	487 ± 78	13
Pentazocine					15.0 ± 3.0	-	-
DTG					-	54 ± 8	-

^a K_i values are given as mean ± SEM of three independent experiments. ^bSelectivity vs. σ_1R was calculated as $K_i\sigma_2R/K_i\sigma_1R$.

2.6. Study of theoretical medicinal chemistry alerts in free databases

Before evaluating the therapeutic potential of the new DFHs in cellular assays, and in order to make an adequate selection of candidates, we studied the potential medicinal chemistry alerts of **1-29** in two free databases, namely ZINC15 (<http://zinc15.docking.org/>) [58] and SwissADME (<http://www.swissadme.ch/>) [59]. According to the ZINC15 web site, none of the hybrids were highlighted as pan assay interference compound (PAINS) or aggregator (see Table S1 in the Supplementary data file). However, in the SwissADME platform three compounds were marked with structural alerts, according to the Brenk method [60]. These compounds were hybrids **14** (nitro group), **15** (aniline derivative) and **19** (catechol), which were consequently discarded for further cellular assays.

2.7. Cell viability and neuroprotective properties

Cell viability and neuroprotective capacity of the new compounds against mitochondrial oxidative stress were evaluated using the human neuroblastoma SH-SY5Y cell line. A toxic cocktail of rotenone (30 μM) and oligomycin A (10 μM) was used as a model of mitochondrial oxidative stress. This mixture of toxic molecules blocks complexes I and V of the respiratory electron transport chain, inducing high concentration of mitochondrial free radicals and cell death, confirming its validity as a good experimental model of mitochondrial oxidative stress [31,38,61-63].

Accordingly, DFH compounds at increasing concentrations (0.1 - 3.0 μM) were co-incubated with the toxic mixture for 24 h; then, cell survival was quantified by the 3-[4,5-dimethylthiazol-2-yl]-2,5-diphenyl-tetrazolium bromide (MTT) colorimetric assay [64]. MTT reduction in basal conditions was considered as 100 % viability of cells

without any treatment. In all experiments, melatonin and donepezil were used as reference drugs, which gave the following percentages of neuroprotection: melatonin (10 nM) = 42.1 ± 3.01 % and donepezil (5 μ M) = 38.4 ± 4.72 %.

For these studies, we selected hybrids with differences in the heterocycle core and in the nature and length of the linker, and without any structural alert (Table 5). To a greater or lesser extent, all tested compounds showed neuroprotective properties against mitochondrial oxidative stress, in especial hybrids **5** (n = 1, X = O, Z = O, R = 6,7-diOMe), **12** (n = 2, X = NH, Z = O, R = 6-OH), **18** (n = 2, X = NH, Z = O, R = 6,7-diOMe), and **24** (n = 2, X = NH, Z = NH, R = 6-OH). The few differences found between ORAC-active and ORAC-inactive compounds (hydroxyl and methoxy hybrids, respectively), suggested that the neuroprotective properties of the new series of DFHs are mainly due to the activation of the endogenous antioxidant response, rather than to the direct capture of radical oxygen species.

Table 5. Neuroprotection (%) of selected DFHs at the indicated concentrations in the human neuroblastoma cell line SH-SY5Y against the cocktail of rotenone (30 μ M) and oligomycin A (10 μ M).

Compd.	n	X	Z	R	0.1 μ M	0.3 μ M	1.0 μ M	3.0 μ M
1	0	NH	O	6-OMe	9.8 \pm 1.1	13.9 \pm 3.1	14.6 \pm 1.2	8.6 \pm 1.7
3	0	NH	O	6,7-diOMe	5.7 \pm 3.6	18.0 \pm 3.1	12.3 \pm 2.5	12.6 \pm 3.1
5	1	O	O	6,7-diOMe	19.4 \pm 0.7*	19.6 \pm 3.0*	6.8 \pm 1.2	12.4 \pm 3.6
12	2	NH	O	6-OH	15.0 \pm 2.9	18.8 \pm 3.8	8.6 \pm 3.0	15.2 \pm 4.9
18	2	NH	O	6,7-diOMe	11.5 \pm 1.5*	18.1 \pm 1.6**	17.1 \pm 1.9*	22.4 \pm 2.5**
24	2	NH	NH	6-OH	18.6 \pm 1.2*	13.7 \pm 5.1*	17.4 \pm 1.3*	29.7 \pm 2.8**

Results are given as mean \pm SEM of 4 independent experiments in triplicate. * $p < 0.05$, ** $p < 0.01$ respect to control. Neuroprotection values of reference drugs: melatonin (10 nM) = 42.1 \pm 3.01 %; donepezil (5 μ M) = 38.4 \pm 4.72 %.

2.8. Neurogenic studies

The brain-permeable 6,7-dimethoxy-4-oxo-4*H*-chromene hybrid **18**, without any structural alert in the online ZINC15 and SwissADME databases, and which displays an interesting *in vitro* profile, namely affinity of σ_1 R, inhibition of human AChE, 5-LOX, MAO-A and MAO-B, and a good neuroprotective activity against mitochondrial oxidative stress, was further evaluated as neurogenic agent. Adult mice neural stem cells (NSC) were isolated from the subgranular zone of the hippocampal dentate gyrus and cultured as neurospheres (NS), which were grown for 7 days in culture with or without compound and then, they were adhered on a substrate to allow differentiation for 3 days [65-67]. Afterward, β -III-tubulin (clone TuJ1) and microtubule-associated protein 2 (MAP-2) antibodies were used to visualize early proliferation and neuronal maturation,

respectively. As shown in Figure 3, derivative **18** clearly promoted the differentiation of NSCs and their further maturation to a neuronal phenotype. Moreover, an important population of these new cells has reached a consolidated neuronal stage, which is indeed observable in their distinctive morphology.

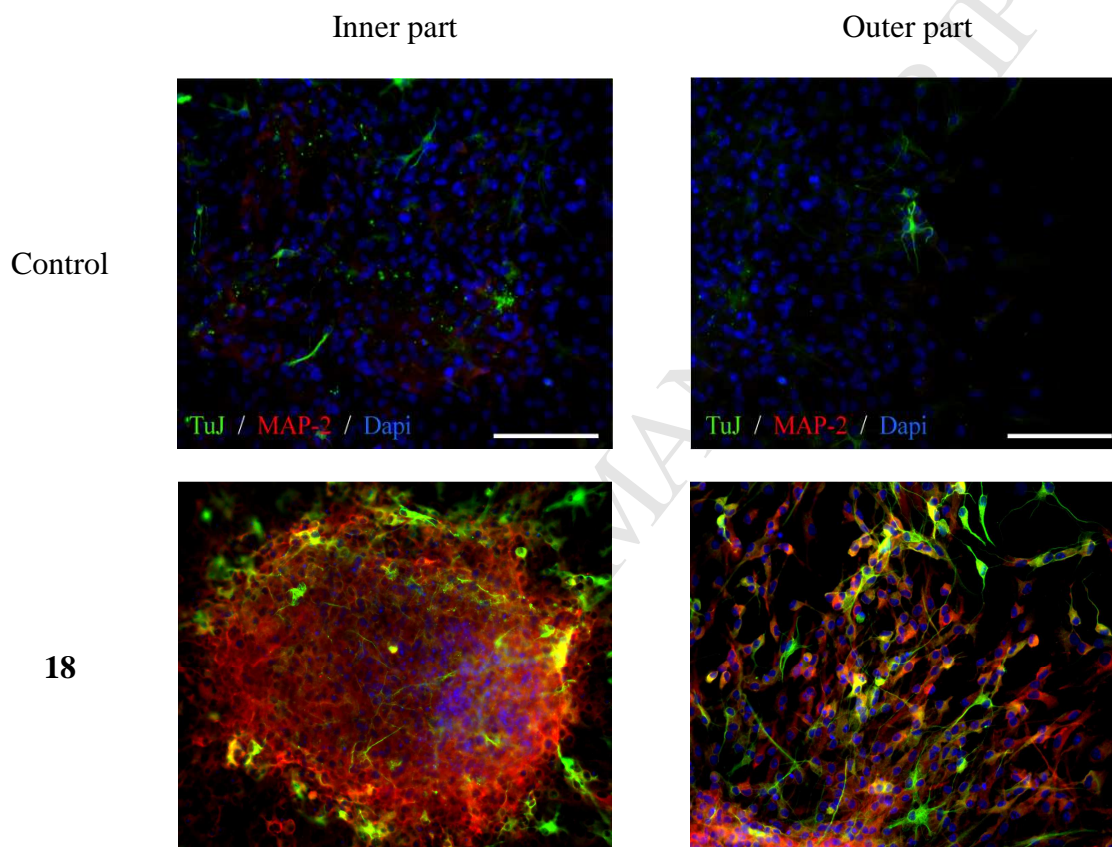


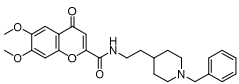
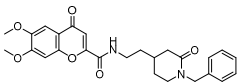
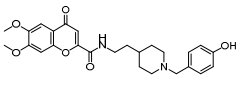
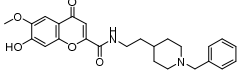
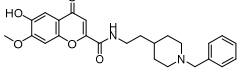
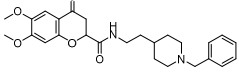
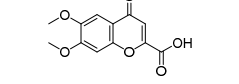
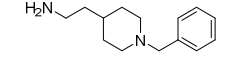
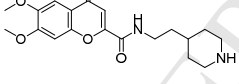
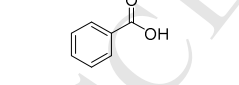
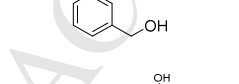
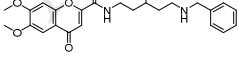
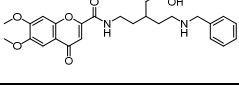
Figure 3. *In vitro* neurogenic effect of hybrid **18** (10 μ M) on mice hippocampal SGZ-derived spheres. NSC enriched spheres were grown for 7 days in culture in the presence of compound (10 μ M). Later on, neurospheres were adhered on a substrate to allow differentiation for 3 days in the presence of compound. Representative images show the expression of β -III-tubulin (TuJ clone; green) and MAP-2 (red) inside the neurosphere (inner part) and in the distal area (outer part). DAPI was used for nuclear staining. Scale bar, 200 μ m.

2.9. *In silico* toxicity and metabolism of hybrid **18**

To study the potential therapeutic success of hybrid **18**, we performed an *in silico* prediction of its toxicity and metabolism in humans using the Nexus knowledge-based system [68]. The toxicity predictions obtained with the Derek Nexus program rely on the comparison of the structural features of a given compound with one or more toxicophore patterns (structural alerts) in the Lhasa's knowledge base 2018 (species: human). There were 55 toxicity endpoints for compound **18**, analyzed at the minimum reasoning level of “impossible” [69] (Chart S1 in Supplementary Information). No alerts were fired for hybrid **18**.

Despite *in silico* structure-activity relationship toxicity models include implicit consideration of metabolism, some metabolic relationships may be missed. Therefore, an *in silico* prediction of the compound metabolism can add value to its toxicological assessment. Hence, we performed a prediction of the most likely phase-I metabolites of hybrid **18**, obtaining 12 structures. Potential toxicity was also assessed for these metabolites with Derek Nexus analyzing 55 endpoints (Chart S1). Again the minimal likelihood to consider a toxic outcome in the analysis was “impossible”. Results showed that the metabolites were not associated with any structural alerts for toxicity by Derek (Table 6).

Table 6. The most possible phase-I metabolites for the hybrid **18** and the associated probable / plausible structural alerts

Compd.	Structure	Bio-transformation name	Phase-I enzyme	Outcome
18		-	-	No alerts fired
M1		Lactams from aza-alicyclic compounds	CYP450	No alerts fired
M2		<i>p</i> -Hydroxylation of monosubstituted benzene compounds	CYP450	No alerts fired
M3		Oxidative <i>O</i> -demethylation	CYP450	No alerts fired
M4		Oxidative <i>O</i> -demethylation	CYP450	No alerts fired
M5		Reduction of α,β -unsaturated compounds	abKDBR	No alerts fired
M6		Hydrolysis of acyclic carboxylic amides	Hydrolase	No alerts fired
M7		Hydrolysis of acyclic carboxylic amides	Hydrolase	No alerts fired
M8		Oxidative <i>N</i> -dealkylation	CYP450	No alerts fired
M9		Oxidative <i>N</i> -dealkylation	CYP450	No alerts fired
M10		Oxidative <i>N</i> -dealkylation	CYP450	No alerts fired
M11		Oxidative <i>N</i> -dealkylation	CYP450	No alerts fired
M12		Oxidative <i>N</i> -dealkylation	CYP450	No alerts fired

CYP450 = cytochrome. abKDBR = α,β -ketoalkene double bond reductases

2.10. Molecular modelling studies on the interactions between hybrid **18** and its biological targets

The 6,7-dimethoxy-4-oxo-4*H*-chromene hybrid **18** is the most characterized and promising compound of all DFHs here described. Indeed, **18** is a good inhibitor of hAChE ($IC_{50} = 46$ nM), a tight σ_1 R binder ($K_i = 37.4$ nM), and it is also moderately active against 5-LOX ($IC_{50} = 74.3$ μ M).

Accordingly, we carried out Molecular Dynamics (MD) simulations to investigate the interactions of **18** with these three target proteins. Initially, the putative binding modes of **18** onto hAChE, 5-LOX, and σ_1 R were identified using a well-validated docking protocol [70]. Next, MD simulations of the resulting **18**/protein complexes were carried out, and the corresponding ligand/protein free energy of binding (ΔG_{bind}) values were obtained via the MM/PBSA (Molecular Mechanics/Poisson-Boltzmann Surface Area) approach [71]. According to the simulations, and in agreement with the corresponding experimental findings, **18** has a strong affinity for both hAChE and σ_1 R, characterized by ΔG_{bind} of -10.03 ± 0.21 kcal/mol and -10.38 ± 0.19 kcal/mol, respectively. Contextually, its moderate 5-LOX inhibitory activity is confirmed by its lower ΔG_{bind} (-5.49 ± 0.22 kcal/mol).

A per-residue binding free energy deconvolution (PRBFED) of the enthalpic terms (ΔH_{res}) was then performed to define and to describe the intermolecular interactions between **18** and the three different proteins (Figure 4).

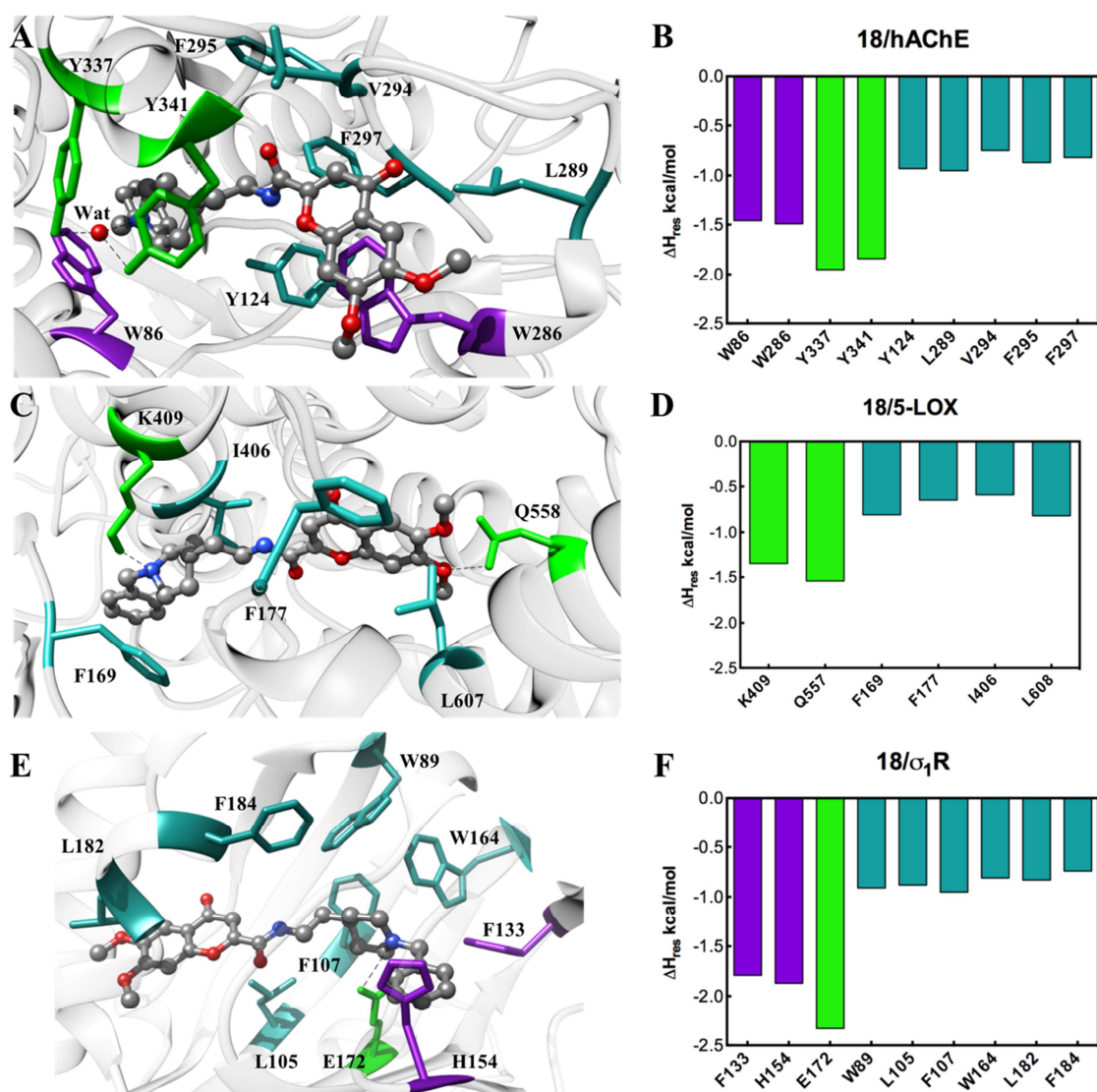


Figure 4. Details of compound **18** in the binding pocket of hAChE (A), 5-LOX (C) and σ_1 R (E). Compound **18** is depicted as atom-coloured sticks-and-balls (C, grey; N, blue; O, red) while the side chains of each protein residues mainly interacting with **18** are highlighted as coloured sticks and labelled. Hydrogen bonds are shown as black broken lines. Hydrogen atoms, water molecules, ions, and counterions are omitted for clarity. Per-residue binding free energy decomposition of the main involved amino acids of **18** in complex with hAChE (B), 5-LOX (D) and σ_1 R (F).

Starting the analysis with the esterase enzyme, the binding mode of **18** (Figure 4A) is fairly similar to that described for donepezil [72]. This is a somewhat expected result, since **18** and the classical hAChE inhibitor share many functional groups and moieties. Accordingly, the piperidine nitrogen atom is engaged in a water-mediated hydrogen bond with the hydroxyl side chain of Y337 ($\Delta H_{\text{res}} = -1.95$ kcal/mol, Figure 4B) and Y341 ($\Delta H_{\text{res}} = -1.84$ kcal/mol) of hAChE. Moreover, the chromene moiety of **18** is involved in a π - π interaction with W286 ($\Delta H_{\text{res}} = -1.49$ kcal/mol), while the *N*-benzyl ring stacks against the side chain of W86 ($\Delta H_{\text{res}} = -1.46$ kcal/mol). Finally, the **18**/hAChE complex is further stabilized in its binding pocket through hydrophobic interactions with the side chains of Y124, L289, V294, F295, and F297 ($\sum \Delta H_{\text{res}} = -4.32$ kcal/mol, Figure 4B).

The interactions between **18** and 5-LOX are definitely less performing, in line with the corresponding binding pose of the chromene derivative in the active site of the receptor. As seen from Figure 4C, the aromatic and hydrophobic portions of **18** are nestled in a cavity surrounded by 5-LOX residues F169, F177, I406, and L608, which afford an overall stabilizing contribution of $\sum \Delta H_{\text{res}} = -2.87$ kcal/mol (Figure 4D). Furthermore, only two further stabilizing interactions are provided by the side chains of K409 ($\Delta H_{\text{res}} = -1.35$ kcal/mol) and Q557 ($\Delta H_{\text{res}} = -1.54$ kcal/mol) as hydrogen bond donors with the **18** acceptor counterparts, i.e., the *N*-piperidine atom and 6-methoxy substituent on the chromene ring.

Finally, the results of the **18**/ σ_1 R complex (Figure 4E) revealed the prototypical pattern of intermolecular interactions underlying σ_1 R ligand binding. Specifically, the basic piperidine nitrogen of **18** is engaged in a persistent salt bridge with the COO⁻ group of E172 ($\Delta H_{\text{res}} = -2.33$ kcal/mol, Figure 4F), whilst the *N*-benzyl ring is aptly

arranged in the binding site trough π - π interaction with the aromatic side chain of F133 ($\Delta H_{\text{res}} = -1.79$ kcal/mol) and H154 ($\Delta H_{\text{res}} = -1.87$ kcal/mol). Finally, the highly hydrophobic σ_1 R binding site assists in nestling the lipophilic moieties of **18**, the 6,7-dimethoxychromene group being perfectly encased in the cavity lined by the side chains of residues W89, L105, F107, and W164, L182, and F184 ($\Sigma\Delta H_{\text{res}} = -5.12$ kcal/mol, Figure 4F).

3. Conclusions

By connecting flavonoid-related structures and a donepezil fragment we have obtained new 4-chromone- and 4-quinolone – *N*-benzylpiperidine hybrids (DFHs) endowed with an interesting phenotypic profile that combines neurogenic and neuroprotective properties in cell-based assays. At the molecular level, these new DFH compounds showed high σ_1 R affinities and good ROS trapping capacities and moreover, they inhibited other key enzymes in AD, such as 5-LOX, AChE and MAOs.

We achieved potent and selective inhibition of human AChE, especially with the 4-chromone series, with IC_{50} from the nanomolar to the low micromolar range, that is, comparable with the donepezil IC_{50} value (10 nM). Hybrids derived from 4-oxo-1*H*-quinoline displayed worse AChE inhibition, probably due to the existence of a tautomeric equilibrium in the azaheterocycle that might be detrimental for the interaction with the enzyme. In the 4-oxo-4*H*-chromene series, the location of substituents in the flavonoid fragment seems to modulate AChE inhibition, as best results were obtained at positions 6 and/or 7, whereas site 5 was unfavourable. Comparing 4-chromone hybrids with a linker of two methylenes ($n = 2$), the most potent

inhibitors could be ranked as: **14** (6-NO₂) > **13** (7-OMe) > **15** (6-NH₂) > **18** (6,7-diOMe) > **12** (6-OH) with IC₅₀s comprised between 21 and 91 nM. Kinetic experiments suggested the simultaneous interaction of the new DFHs with the two main sites of the AChE gorge (CAS and PAS).

According to the well-known *in vitro* PAMPA-BBB model, the majority of new 4-chromone-, and quinoline-based hybrids could enter into the CNS by passive diffusion, and only some hydroxyl derivatives (**2**, **12**, **17**, and **19**) were predicted to have difficulties to pass the BBB.

Regarding 5-LOX inhibition, 4-quinolone derivatives were worse than 4-chromone hybrids, in which the type, amount, and position of substituents reflected in major differences in potency. In general, di-hydroxyl compounds were better 5-LOX inhibitors than chromones bearing only one hydroxyl group, 6,7-positions being preferred.

Several DFHs were determined to be micromolar inhibitors of human MAO-A and MAO-B, with IC₅₀s similar to drugs used in the clinic, such as iproniazid and moclobemide. In the ORAC experiments, better antioxidant properties were obtained with hydroxyl-derived hybrids.

In relation to σ_1 R / σ_2 R interactions, all tested hybrids showed a net selectivity for the subtype σ_1 R with K_i s in the nano- and subnanomolar range. Best σ_1 R affinity values were achieved with a hydrogen-bond acceptor group in the position 6 of the heterocycle, whereas substituents at positions 7 and 8 decreased receptor affinity.

Molecular modelling studies of hybrid **18** in AChE, 5-LOX and σ_1 R have shown the key interactions with these proteins and have provided a rationale about the

experimental values obtained: nanomolar values for both hAChE inhibition and σ_1 R affinity, and micromolar inhibition of 5-LOX.

Our new hybrids provided protection against mitochondrial oxidative stress through a mechanism that likely implies the activation of the endogenous antioxidant response, instead of the direct capture of ROS. In neurogenic assays, *N*-(2-(1-benzylpiperidin-4-yl)ethyl)-6,7-dimethoxy-4-oxo-4*H*-chromene-2-carboxamide (**18**) stimulated the differentiation of stem-cells derived from the SGZ of adult mice to a neuronal phenotype. Thereby, this donepezil-flavonoid hybrid could contribute to the endogenous auto-repair processes of the CNS. Furthermore, the safety profile obtained from the *in silico* predictions makes hybrid **18** a molecule of potential interest in the quest for effective agents against AD and other NDs.

4. Experimental section

4.1. Chemistry. General methods

Reagents and solvents were purchased from common commercial suppliers (mostly Sigma-Aldrich) and were used without further purification. Thin-layer chromatography (TLC) was carried out using Merck silica gel 60 F254 plates and compounds were visualized under UV-light ($\lambda = 254$ or 365 nm) and/or stained with phosphomolybdic acid 10% wt. in ethanol. Automatized chromatographic separation was carried out with an IsoleraOne (Biotage) equipment, using different silica Biotage ZIP KP-Sil 50μ cartridges. High-performance liquid chromatography was performed on a Waters analytical HPLC-MS (Alliance Watters 2690) equipped with a SunFire C_{18} 4.6×50 mm column, a UV photodiode array detector ($\lambda = 214$ – 274 nm) and quadrupole mass spectrometer (Micromass ZQ). HPLC analyses were used to confirm the purity of all compounds ($\geq 95\%$) and were performed on Waters 6000 equipment, at a flow rate of 1.0 mL/min, with a UV photodiode array detector ($\lambda = 214$ – 274 nm), and using a Delta Pak C_{18} $5 \mu\text{m}$, 300 \AA column. Elution was performed in a gradient mixture of ACN/water, starting in most of cases with 15% and ending with 95% of ACN within a gradient time (g.t.) of 5 minutes (Water - ACN (15 \rightarrow 95%), g.t. 5 min). Melting points (uncorrected) were determined with a MP70 apparatus (Mettler Toledo). ^1H NMR and ^{13}C NMR spectra were obtained in MeOD, DMSO- d_6 CDCl_3 or CD_3OD solutions using the following NMR spectrometers: Varian INOVA-300, Varian INOVA-400, Varian Mercury-400 or Varian Unity-500. Chemical shifts are reported in δ scale (ppm) relative to internal Me_4Si . J values are given in Hertz, and spin multiplicities are expressed as s (singlet), broad signal (bs), d (doublet), t (triplet), q (quartet), or m (multiplet). High resolution mass spectrometry (HRMS) data were obtained by electron spray ionization in positive mode (ESI $^+$) using a Hewlett-Packard MSD 1100 spectrometer.

4.2. General procedure for the synthesis of chromene - N-benzylpiperidine hybrids using 1,1'-carbonyldiimidazole (CDI) as coupling agent (method A)

The corresponding 4-oxo-4*H*-chromene-2-carboxylic acid (1.0 mmol) and 1,1'-carbonyldiimidazole (CDI, 1.3 mmol) were mixed into a 10 mL microwave vial under N₂ atmosphere. The vial was sealed and 5 mL of anhydrous DMF were added using a syringe to dissolve the mixture (CO₂↑). This solution was heated into a microwave reactor at 120 °C during 10 min to complete the activation of the acid. Afterward, the corresponding amine (1.2 mmol) dissolved in 2 mL of DMF was added with a syringe, and the mixture was heated again during 10 min at 150 °C to obtain the desired amide. After completion of the reaction, the DMF was evaporated under reduced pressure; the crude material was re-dissolved in 25 mL of EtOAc and washed with water (3 x 5 mL) and brine (3 x 5 mL), dried over MgSO₄ and concentrated. The product was purified by column chromatography using EtOAc:MeOH (9:1) as eluent.

4.3. General procedure for the synthesis of chromene - N-benzylpiperidine hybrids using benzotriazol-1-yloxy-tris(dimethylamino)phosphonium hexafluorophosphate (BOP) as coupling agent (method B)

Into a round-bottom flask, the corresponding acid (1.0 mmol) was dissolved with 10 mL of anhydrous DMF under N₂ atmosphere; to this mixture, BOP (3 mmol) was added and stirred during 5 min; subsequently, triethylamine (2.5 mmol) was added to dissolve utterly the reagents. The mixture was stirred again during 5 min and finally, the corresponding amine (1.1 mmol) was added to stir overnight at room temperature. The mixture of reaction was washed with HCl (0.5 M) (3 x 5 mL), saturated solution of NaHCO₃ (3 x 5 mL) and brine (3 x 5 mL), dried over MgSO₄, filtered and concentrated. The crude was purified by column chromatography using EtOAc/MeOH (9:1) as eluent.

4.4. General procedure for the synthesis of hydroxyl derivatives (method C)

Under N₂ atmosphere and over an ice bath, to a solution of the corresponding methoxy hybrid (0.1 mmol) in anhydrous dichloromethane (DCM, 3 mL), BBr₃ (1 equivalent per each heteroatom present in the molecule) was added slowly under magnetic stirring. The mixture was allowed to react overnight at room temperature and then, quenched with MeOH (dropwise until end of effervescence). Solvent was evaporated under reduced pressure and residue was purified by column chromatography using a gradient of EtOAc/MeOH 0→10% as eluent.

4.5. General procedure for the synthesis of 6-amino-N-(2-(1-benzylpiperidin-4-yl)ethyl)-4-oxo-4H-chromene-2-carboxamide (**15**) (method D)

To a solution of the nitro derivative **14** (0.2 g 0.46 mmol) in EtOH (5 mL), a catalytic amount of Pd/charcoal 5% was added under N₂ atmosphere. Subsequently, N₂ was displaced by H₂ and the flask was sealed up with a rubber septum. Then, a balloon containing H₂ was connected with a needle through the septum to stir overnight at 30 °C. Once reaction was completed, the catalyzer was eliminated by filtration and the solvent evaporated under reduced pressure. Residue was purified by column chromatography using a gradient of EtOAc/MeOH 0→10% as eluent

4.6. General procedure for the synthesis of dihydroquinoline - N-benzylpiperidine hybrids (method E)

Under N₂ atmosphere, Al(CH₃)₃ (2M in heptane, 3.0 mmol) was injected with a syringe into a mixture of the corresponding methyl 4-oxo-1,4-dihydroquinoline-2-

carboxylate (or methyl 4,6,7-trimethoxyquinoline-2-carboxylate for the synthesis of **29**) (1.0 mmol) and 2-(1-benzylpiperidin-4-yl)ethan-1-amine (1.0 mmol) in dry THF (3.5 mL) in a microwave vial. This mixture was heated into a microwave reactor at 120 °C for 1.5 min; then, the crude was treated with HCl 2M (dropwise) until the end of effervescence, neutralized with NaOH 2M and the liquid phase evaporated to dryness. The solid was washed with EtOAc (5 x 5.0 mL) and methanol (2 x 5.0 mL) and these fractions were mixed and concentrated under reduced pressure. The product was purified by column chromatography using a gradient of EtOAc in hexane (0→65%) as eluent.

4.7. Chemical description of hybrids **1-29**

4.7.1. *N*-(1-Benzylpiperidin-4-yl)-6-methoxy-4-oxo-4*H*-chromene-2-carboxamide (**1**)

Following method A, from 6-methoxy-4-oxo-4*H*-chromene-2-carboxylic acid [53] (0.20 g, 0.9 mmol) and 1-benzylpiperidin-4-amine (0.19 g, 1.0 mmol), hybrid **1** (0.25 g, 70% yield) was obtained as a white solid of mp 196 - 199 °C. ¹H NMR (300 MHz, MeOD) δ 7.72 (d, *J* = 9.2 Hz, 1H, H₈), 7.53 (d, *J* = 3.1 Hz, 1H, H₅), 7.46 (dd, *J* = 9.2, 3.1 Hz, 1H, H₇), 7.38 – 7.28 (m, 5H, Ph), 6.96 (s, 1H, H₃), 3.92 (s, 4H, H_{4'}, _{61'}), 3.58 (s, 2H, H_γ), 2.99 (d, *J* = 11.9 Hz, 2H, H_{2'eq}), 2.20 (td, *J* = 11.9, 2.5 Hz, 2H, H_{2'ax}), 2.03 – 1.88 (m, 2H, H_{3'eq}), 1.78 (tt, *J* = 13.3, 6.6 Hz, 2H, H_{3'ax}). ¹³C NMR (75 MHz, MeOD) δ 180.23 (C₄), 160.81 (C₉), 159.21 (C₆), 157.30 (C₂), 151.86 (C_{8a}), 138.52 (C_i), 130.73 (C_o), 129.33 (C_m), 128.47 (C_p), 125.88 (C₇), 125.83 (C_{4a}), 121.37 (C₈), 111.08 (C₃), 105.68 (C₅), 63.93 (C_γ), 56.42 (C₆₁), 53.53 (C_{2'}), 49.17 (C_{4'}) 32.04 (C_{3'}). HRMS [ESI+] *m/z* = 392.1742 [M]⁺, calcd for [C₂₃H₂₄N₂O₄]⁺ 392.1736. HPLC purity 100%.

4.7.2. *N*-(1-Benzylpiperidin-4-yl)-6-hydroxy-4-oxo-4*H*-chromene-2-carboxamide (**2**)

Following method C, from **1** (0.05 g, 0.013 mmol) and BBr₃ (0.1 mmol), hybrid **2** was obtained (0.013 g, 70% yield), as a white solid of mp 302 - 304 °C. ¹H NMR (500 MHz, MeOD) δ 7.65 (d, *J* = 9.1 Hz, 1H, H₈), 7.56 – 7.51 (m, 5H, Ph), 7.43 (d, *J* = 3.0 Hz, 1H, H₅), 7.34 (dd, *J* = 9.1, 3.0 Hz, 1H, H₇), 6.94 (s, 1H, H₃), 4.35 (s, 2H, H_γ), 4.25 – 4.15 (m, 1H, H_{4'}), 3.66 – 3.50 (m, 2H, H_{2'eq}), 3.25 – 3.13 (m, 2H, H_{2'ax}), 2.29 – 2.17 (m, 2H, H_{3'eq}), 2.09 – 1.96 (m, 2H, H_{3'ax}). ¹³C NMR (126 MHz, MeOD) δ 180.33 (C₄), 161.28 (C₉), 157.26 (C_{8a}), 156.84 (C₂), 150.97 (C₆), 132.35 (C_o), 131.33 (C_p), 130.44 (C_m), 130.44 (C_i), 126.06 (C_{4a}), 125.59 (C₇), 121.13 (C₈), 110.96 (C₃), 108.72 (C₅), 61.88 (C_γ), 52.86 (C_{2'}), 29.75 (C_{3'}). HRMS [ESI+] *m/z* = 378.15814 [M]⁺, calcd for [C₂₂H₂₂N₂O₄]⁺ 378.1579. HPLC purity 97%.

4.7.3. *N*-(1-Benzylpiperidin-4-yl)-6,7-dimethoxy-4-oxo-4*H*-chromene-2-carboxamide

(**3**)

Following method B, from 6,7-dimethoxy-4-oxo-4*H*-chromene-2-carboxylic acid [53] (0.05 g, 0.20 mmol) and 1-benzylpiperidin-4-amine (0.42 g, 0.22 mmol), hybrid **3** was obtained (0.04 g, 54% yield), as a white solid of mp 183-185 °C. ¹H NMR (300 MHz, MeOD) δ 7.45 (s, 1H, H₈), 7.42 – 7.29 (m, 5H, Ph), 7.26 (s, 1H, H₅), 6.93 (s, 1H, H₃), 4.01 (s, 3H, H₇₁), 3.98 – 3.83 (m, 4H, H_{4',61}), 3.65 (s, 2H, H_γ), 3.05 (d, *J* = 11.9 Hz, 2H, H_{2'eq}), 2.36 – 2.21 (m, 2H, H_{2'ax}), 2.06 – 1.93 (m, 2H, H_{3'eq}), 1.90 – 1.70 (m, 2H, H_{3'ax}). ¹³C NMR (75 MHz, MeOD) δ 179.42 (C₄), 160.78 (C₉), 157.36 (C₇), 156.75 (C₂), 153.43 (C_{8a}), 150.02 (C₆), 137.96 (C_i), 130.85 (C_o), 129.41 (C_m), 128.67 (C_p), 118.40 (C_{4a}), 111.38 (C_{4'}), 104.68 (C₈), 101.31 (C₅), 63.76 (C_γ), 57.07 (C₇₁), 56.66

(C₆₁), 53.44 (C_{2'}), 31.89 (C_{3'}). HRMS [ESI+] m/z =422.1850 [M]⁺, calcd for [C₂₄H₂₆N₂O₅]⁺ 422.1842. HPLC purity 97%.

4.7.4. (1-Benzylpiperidin-4-yl)methyl 6-methoxy-4-oxo-4H-chromene-2-carboxylate (**4**)

Following method A, from 6-methoxy-4-oxo-4H-chromene-2-carboxylic acid [53] (0.05 g, 0.23 mmol) and (1-benzylpiperidin-4-yl)methanol (0.055 g, 0.27 mmol), hybrid **4** was obtained (0.11 g, 12% yield), as a white solid of mp 185 -188 °C. ¹H NMR (500 MHz, CDCl₃) δ 7.64 – 7.60 (m, 3H, H_{o, 8}), 7.52 (d, J = 3.2 Hz, 1H, H₅), 7.47 – 7.44 (m, 3H, H_{m, p}), 7.34 (dd, J = 9.2, 3.2 Hz, 1H, H₇), 7.05 (s, 1H, H₃), 4.30 (d, J = 6.3 Hz, 2H, H_α), 4.17 (s, 2H, H_γ), 3.89 (s, 3H, H₆₁), 3.54 (d, J = 12.1 Hz, 2H, H_{2'eq}), 2.70 – 2.61 (m, 2H, H_{2'ax}), 2.38 – 2.24 (m, 2H, H_{3'eq}), 2.08 – 1.87 (m, 3H, H_{3'ax, 4'}). ¹³C NMR (126 MHz, CDCl₃) δ 178.26 (C₄), 160.46 (C₉), 157.74 (C₆), 151.49 (C₂), 150.97 (C_{8a}), 131.64 (C_o), 130.43 (C_p), 129.53 (C_m), 127.93 (C_i), 125.32 (C₇), 120.59 (C₈), 120.40 (C_{4a}), 114.17 (C₃), 104.66 (C₅), 69.30 (C_α), 61.23 (C_γ), 56.12 (C₆₁), 51.85 (C_{2'}), 33.85 (C_{4'}), 25.76 (C_{3'}). HRMS [ESI+] m/z =407.1741 [M]⁺, calcd for [C₂₄H₂₅NO₅]⁺ 407.1733. HPLC purity 98%.

4.7.5. (1-Benzylpiperidin-4-yl)methyl 6,7-dimethoxy-4-oxo-4H-chromene-2-carboxylate (**5**)

Following method B, from 6,7-dimethoxy-4-oxo-4H-chromene-2-carboxylic acid [53] (0.05 g, 0.20 mmol) and (1-benzylpiperidin-4-yl)methanol (0.05 g, 0.24 mmol), hybrid **5** was obtained (0.035 g, 40% yield), as a white solid of mp 138 -140 °C. ¹H NMR (500 MHz, CDCl₃) δ 7.65 – 7.60 (m, 2H, H_o), 7.48 (s, 1H, H₈), 7.48 – 7.42 (m, 3H, H_{m, p}), 7.33 (s, 1H, H₅), 7.06 (s, 1H, H₃), 4.30 (d, J = 5.4 Hz, 2H, H_α), 4.18 (s, 2H,

H_γ), 4.06 (s, 3H, H₇₁), 3.97 (s, 3H, H₆₁), 3.59 – 3.53 (m, 2H, H_{2'eq}), 2.75 – 2.63 (m, 2H, H_{2'ax}), 2.49 – 2.34 (m, 2H, H_{3'eq}), 2.04 – 1.97 (m, 1H, H_{4'}), 1.97 – 1.91 (m, 2H, H_{3'ax}). ¹³C NMR (126 MHz, CDCl₃) δ 177.34 (C₄), 160.64 (C₉), 155.79 (C₇), 152.57 (C_{8a}), 151.13 (C₂), 148.55 (C₆), 131.63 (C_o), 130.46 (C_p), 129.55 (C_m), 127.91 (C_i), 118.21 (C_{4a}), 114.71 (C₃), 103.93 (C₈), 101.00 (C₅), 69.04 (C_α), 61.23 (C_γ), 57.31 (C₇₁), 56.53 (C₆₁), 51.97 (C_{2'}), 33.78 (C_{4'}), 25.69 (C_{3'}). HRMS [ESI+] *m/z* = 437.1859 [M]⁺, calcd for [C₂₅H₂₇NO₆]⁺ 437.1838. HPLC purity 97%.

4.7.6. *N-((1-Benzylpiperidin-4-yl)methyl)-6-methoxy-4-oxo-4H-chromene-2-carboxamide (6)*

Following method A, from 6-methoxy-4-oxo-4H-chromene-2-carboxylic acid [53] (0.05 g, 0.23 mmol) and (1-benzylpiperidin-4-yl)methanamine (0.051 g, 0.25 mmol), hybrid **6** (0.055 g, 60% yield) was obtained as a white solid of mp 116 -118 °C. ¹H NMR (500 MHz, CDCl₃) δ 7.55 (d, *J* = 3.1 Hz, 1H, H₅), 7.42 (d, *J* = 9.1 Hz, 1H, H₈), 7.31 – 7.20 (m, 6H, Ph, H₇), 7.12 (s, 1H, H₃), 6.90 (t, *J* = 6.2 Hz, 1H, NH), 3.88 (s, 3H, H₆₁), 3.48 (s, 2H, H_γ), 3.37 (t, *J* = 6.2 Hz, 2H, H_α), 2.90 (d, *J* = 11.4 Hz, 2H, H_{2'eq}), 1.96 (dt, *J* = 11.4, 6.1 Hz, 2H, H_{2'ax}), 1.71 (d, *J* = 12.7 Hz, 2H, H_{3'eq}), 1.67 – 1.50 (m, 1H, H_{4'}), 1.45 – 1.26 (m, 2H, H_{3'ax}). ¹³C NMR (126 MHz, CDCl₃) δ 178.14 (C₄), 159.58 (C₉), 157.65 (C₆), 154.59 (C₂), 150.08 (C_{8a}), 138.42 (C_i), 129.33 (C_o), 128.34 (C_m), 127.17 (C_p), 125.23 (C_{4a}), 124.77 (C₇), 119.56 (C₈), 111.46 (C₃), 105.28 (C₅), 63.45 (C_γ), 56.16 (C₆₁), 53.36 (C_{3'}), 45.56 (C_α), 36.17 (C_{4'}), 30.12 (C_{2'}). HRMS [ESI+] *m/z* = 406.1908 [M]⁺, calcd for [C₂₄H₂₆N₂O₄]⁺ 406.1893. HPLC purity 98%.

4.7.7. *N-((1-Benzylpiperidin-4-yl)methyl)-6,7-dimethoxy-4-oxo-4H-chromene-2-carboxamide (7)*

Following method B, from 6,7-dimethoxy-4-oxo-4*H*-chromene-2-carboxylic acid [53] (0.20 g, 0.80 mmol) and (1-benzylpiperidin-4-yl)methanamine (0.18 g, 0.88 mmol), hybrid **7** was obtained (0.17 g, 50% yield), as a white solid of mp 172 - 174 °C. ¹H NMR (500 MHz, MeOD) δ 7.44 (s, 1H, H₅), 7.35 – 7.24 (m, 5H, Ph), 7.20 (s, 1H, H₈), 6.92 (s, 1H, H₃), 3.99 (s, 3H, H₇₁), 3.92 (s, 3H, H₆₁), 3.56 (s, 2H, H_γ), 3.33 (bs, 2H, H_α), 2.97 (dt, *J* = 12.0, 3.2 Hz, 2H, H_{2'eq}), 2.08 (td, *J* = 12.0, 2.5 Hz, 2H, H_{2'ax}), 1.84 – 1.76 (m, 2H, H_{3'eq}), 1.72 (tq, *J* = 7.6, 3.7 Hz, 1H, H_{4'}), 1.43 – 1.32 (m, 2H, H_{3'ax}). ¹³C NMR (126 MHz, MeOD) δ 179.44 (C₄), 161.50 (C₉), 157.37 (C₇), 156.74 (C₂), 153.41 (C_{8a}), 150.03 (C₆), 137.97 (C_i), 130.92 (C_o), 129.32 (C_m), 128.55 (C_p), 118.37 (C_{4a}), 111.34 (C₃), 104.68 (C₅), 101.22 (C₈), 64.17 (C_γ), 57.06 (C₇₁), 56.66 (C₆₁), 54.25 (C_{2'}), 46.23 (C_α), 37.06 (C_{4'}), 30.50 (C_{3'}). HPLC-MS (Water-ACN 2→95%, g.t. 10 min), retention time 6.27 min, *m/z* = 437.2 [M + H]⁺, calcd for [C₂₅H₂₈N₂O₅ + H]⁺ 437.2. HPLC purity 100%.

4.7.8. *2-(1-Benzylpiperidin-4-yl)ethyl 6,7-dimethoxy-4-oxo-4H-chromene-2-carboxylate (8)*

Following method B, from 6,7-dimethoxy-4-oxo-4*H*-chromene-2-carboxylic acid [53] (0.20 g, 0.80 mmol) and 2-(1-benzylpiperidin-4-yl)ethan-1-ol (0.191 g, 0.88 mmol), hybrid **8** was obtained (0.29 g, 80% yield), as a white solid of mp 129 -130 °C. ¹H NMR (500 MHz, CDCl₃) δ 7.51 (s, 1H, H₈), 7.39 – 7.24 (m, 5H, Ph), 7.06 (s, 1H, H₃), 7.03 (s, 1H, H₅), 4.43 (t, *J* = 6.6 Hz, 2H, H_α), 3.99 (s, 3H, H₇₁), 3.98 (s, 3H, H₆₁), 3.60 (s, 2H, H_γ), 2.99 (s, 2H, H_{2'eq}), 2.15 – 1.99 (m, 2H, H_{2'ax}), 1.82 – 1.67 (m, 4H,

H_{3'}eq, β), 1.53 – 1.24 (m, 3H, H_{3'}ax, 4'). ¹³C NMR (126 MHz, CDCl₃) δ 177.49 (C₄), 160.77 (C₉), 155.52 (C₇), 152.42 (C_{8a}), 151.46 (C₂), 148.48 (C₆), 129.70 (C_o), 129.14 (C_i), 128.51 (C_m), 126.20 (C_p), 118.31 (C_{4a}), 114.61 (C₃), 104.19 (C₈), 100.33 (C₅), 64.83 (C_α), 63.15 (C_γ), 56.80 (C₇₁), 56.57 (C₆₁), 53.50 (C_{2'}), 35.00 (C_β), 32.53 (C_{4'}), 29.85 (C_{3'}). HRMS [ESI+] *m/z* =451.2005 [M]⁺, calcd for [C₂₆H₂₉NO₆]⁺ 451.1995. HPLC purity 96%.

4.7.9. *N*-(2-(1-Benzylpiperidin-4-yl)ethyl)-4-oxo-4*H*-chromene-2-carboxamide (**9**)

Following method A, from 4-oxo-4*H*-chromene-2-carboxylic acid (0.20 g, 1.0 mmol) and 2-(1-benzylpiperidin-4-yl)ethan-1-amine (0.275 g, 1.20 mmol), hybrid **9** was obtained (0.50 g, 97% yield), as a white solid of mp 163 - 165 °C. ¹H NMR (300 MHz, MeOD) δ 8.14 (dd, *J* = 8.1, 1.7 Hz, 1H, H₅), 7.85 (ddd, *J* = 8.6, 7.1, 1.7 Hz, 1H, H₆), 7.72 (dd, *J* = 8.6, 1.2 Hz, 1H, H₈), 7.52 (ddd, *J* = 8.1, 7.1, 1.2 Hz, 1H, H₇), 7.42 – 7.22 (m, 5H, Ph), 6.97 (s, 1H, H₃), 3.52 (s, 2H, H_γ), 3.45 (t, *J* = 7.4 Hz, 2H, H_α), 2.91 (d, *J* = 11.5 Hz, 2H, H_{2'}eq), 2.05 (t, *J* = 11.4 Hz, 2H, H_{2'}ax), 1.78 (d, *J* = 12.3 Hz, 2H, H_{3'}eq), 1.67 – 1.53 (m, 2H, H_β), 1.45 – 1.18 (m, 3H, H_{3'}ax, 4'). ¹³C NMR (126 MHz, MeOD) δ 180.43 (C₄), 161.24 (C₉), 157.52 (C₂), 157.13 (C_{8a}), 138.01 (C_i), 136.31 (C₆), 130.97 (C_o), 129.29 (C_m), 128.51 (C_p), 127.29 (C₇), 126.37 (C₅), 125.07 (C_{4a}), 119.81 (C₈), 111.88 (C₃), 64.29 (C_γ), 54.60 (C_{2'}), 38.64 (C_α), 36.90 (C_β), 34.47 (C_{4'}), 32.66 (C_{3'}). HRMS [ESI+] *m/z* =390.1944 [M]⁺, calcd for [C₂₄H₂₆N₂O₃]⁺ 390.1943. HPLC purity 100%.

4.7.10. *N*-(2-(1-Benzylpiperidin-4-yl)ethyl)-5-methoxy-4-oxo-4*H*-chromene-2-carboxamide (**10**)

Following method A, from 5-methoxy-4-oxo-4*H*-chromene-2-carboxylic acid [73] (0.22 g, 1.0 mmol) and 2-(1-benzylpiperidin-4-yl)ethan-1-amine (0.26 g, 1.2 mmol), hybrid **10** was obtained (0.35 g, 84% yield) as a pale syrup. ¹H NMR (500 MHz, MeOD) δ 7.75 (t, *J* = 8.4 Hz, 1H, H₇), 7.62 – 7.52 (m, 2H, H_o), 7.51 – 7.30 (m, 3H, H_m, *p*), 7.26 (dt, *J* = 8.5, 1.1 Hz, 1H, H₆), 7.05 (dd, *J* = 8.5, 0.9 Hz, 1H, H₈), 6.84 (s, 1H, H₃), 4.37 (s, 2H, H_γ), 3.95 (s, 3H, H₅₁), 3.53 – 3.41 (m, 2H, H_α), 3.16 – 3.09 (m, 2H, H_{2'eq}), 2.92 – 2.80 (m, 2H, H_{2'ax}), 1.69 – 1.56 (m, 2H, H_β), 1.39 – 1.35 (m, 1H, H_{4'}), 1.34 – 1.26 (m, 2H, H_{3'eq}), 1.06 – 0.92 (m, 2H, H_{3'ax}). ¹³C NMR (126 MHz, MeOD) δ 163.16 (C₄), 161.09 (C₁), 161.07 (C₅), 159.01 (C_{8a}), 155.55 (C₂), 136.67 (C₇), 134.11 (C_o), 131.00 (C_i), 130.65 (C_p), 129.42 (C_m), 115.42 (C_{4a}), 113.47 (C₃), 111.31 (C₆), 108.57 (C₈), 76.03 (C_γ), 64.63 (C_{3'}), 56.75 (C₅₁), 38.26 (C_σ), 36.44 (C_β), 32.59 (C_{3'}), 30.42 (C_{4'}). HRMS [ESI+] *m/z* = 420.2068 [M]⁺, calcd for [C₂₅H₂₈N₂O₄]⁺ 420.2049. HPLC purity 96%.

4.7.11. *N*-(2-(1-Benzylpiperidin-4-yl)ethyl)-6-methoxy-4-oxo-4*H*-chromene-2-carboxamide (**11**)

Following method A, from 6-methoxy-4-oxo-4*H*-chromene-2-carboxylic acid [53] (0.15 g, 0.70 mmol) and 2-(1-benzylpiperidin-4-yl)ethan-1-amine (0.18 g, 0.82 mmol), hybrid **11** (0.23 g, 80% yield) was obtained as a white solid of mp 137-139 °C. ¹H NMR (300 MHz, CDCl₃) δ 7.69 (d, *J* = 3.1 Hz, 1H, H₅), 7.57 (d, *J* = 9.2 Hz, 1H, H₇), 7.47 – 7.32 (m, 6H, Ph, H₈), 7.26 (s, 1H, H₃), 7.00 (t, *J* = 5.0 Hz, 1H, NH), 4.02 (s, 3H, H₆₁), 3.69 – 3.59 (m, 4H, H_{α, γ}), 3.02 (d, *J* = 10.7 Hz, 2H, H_{2'eq}), 2.10 (t, *J* = 10.7 Hz, 2H,

H_{2'}ax), 1.84 (d, $J = 9.5$ Hz, 2H, H_{3'}eq), 1.73 (p, $J = 6.1$ Hz, 2H, H_β), 1.57 – 1.38 (m, 3H, H_{3'}ax, 4'). ¹³C NMR (75 MHz, CDCl₃) δ 178.14 (C₄), 159.39 (C₉), 157.63 (C₆), 154.65 (C₂), 150.09 (C_{8a}), 138.28 (C_i), 129.40 (C_o), 128.30 (C_m), 127.14 (C_p), 125.20 (C_{4a}), 124.72 (C₈), 119.54 (C₇), 111.33 (C₃), 105.26 (C₅), 63.52 (C_γ), 56.13 (C₆₁), 53.74 (C_{2'}), 37.91 (C_α), 36.29 (C_β), 33.69 (C_{4'}), 32.23 (C_{3'}). HRMS [ESI+] $m/z = 420.2068$ [M]⁺, calcd for [C₂₅H₂₈N₂O₄]⁺ 420.2049. HPLC purity 100%.

4.7.12. *N*-(2-(1-Benzylpiperidin-4-yl)ethyl)-6-hydroxy-4-oxo-4H-chromene-2-carboxamide (**12**)

Following method C, from derivative **11** (0.05 g, 0.12 mmol) and BBr₃ (0.3 g, 1.2 mmol), hybrid **12** was obtained (0.045 g, 93% yield) as a pale yellow solid of mp 204.5 (desc.) °C. ¹H NMR (500 MHz, MeOD) δ 7.67 (d, $J = 9.1$ Hz, 1H, H₈), 7.55 – 7.52 (m, 2H, H_o), 7.50 – 7.47 (m, 3H, H_{m, p}), 7.43 (d, $J = 2.9$ Hz, 1H, H₅), 7.34 (dd, $J = 9.1, 2.9$ Hz, 1H, H₇), 6.94 (s, 1H, H₃), 4.26 (s, 2H, H_γ), 3.50 (t, $J = 6.8$ Hz, 2H, H_α), 3.43 (d, $J = 12.5$ Hz, 2H, H_{2'}eq), 2.97 (t, $J = 12.5$ Hz, 2H, H_{2'}ax), 2.06 (d, $J = 13.4$ Hz, 2H, H_{3'}eq), 1.77 – 1.70 (m, 1H, H_{4'}), 1.67 (q, $J = 6.8$ Hz, 2H, H_β), 1.59 – 1.48 (m, 2H, H_{3'}ax). ¹³C NMR (126 MHz, MeOD) δ 180.43 (C₄), 161.54 (C₉), 157.21 (C_{8a}), 157.07 (C₂), 150.98 (C₆), 132.26 (C_o), 131.19 (C_i), 130.94 (C_p), 130.23 (C_m), 125.98 (C_{4a}), 125.54 (C₇), 121.21 (C₈), 110.73 (C₃), 108.71 (C₅), 61.73 (C_γ), 53.51 (C_{2'}), 38.09 (C_α), 36.09 (C_β), 32.39 (C_{4'}), 30.34 (C_{3'}). HRMS [ESI+] $m/z = 406.1893$ [M]⁺, calcd for [C₂₄H₂₆N₂O₄]⁺ 406.1893. HPLC purity 99%.

4.7.13. *N*-(2-(1-Benzylpiperidin-4-yl)ethyl)-7-methoxy-4-oxo-4*H*-chromene-2-carboxamide (**13**)

Following method A, from 7-methoxy-4-oxo-4*H*-chromene-2-carboxylic acid [74] (0.22 g, 1.0 mmol) and 2-(1-benzylpiperidin-4-yl)ethan-1-amine (0.26 g, 1.2 mmol), hybrid **13** was obtained (0.38 g, 90% yield) as a white solid of mp 141 - 143 °C. ¹H NMR (500 MHz, MeOD) δ 7.99 (d, *J* = 8.9 Hz, 1H, H₅), 7.32 – 7.29 (m, 4H, H_{o, m}), 7.25 (ddd, *J* = 8.9, 5.0, 3.8 Hz, 1H, H_p), 7.13 (d, *J* = 2.4 Hz, 1H, H₈), 7.06 (dd, *J* = 8.9, 2.4 Hz, 1H, H₆), 6.88 (s, 1H, H₃), 3.94 (s, 3H, H₇₁), 3.51 (s, 2H, H_γ), 3.44 (dd, *J* = 8.1, 6.6 Hz, 2H, H_α), 2.90 (dt, *J* = 12.1, 3.3 Hz, 3H, H_{2'eq}), 2.03 (td, *J* = 11.7, 2.5 Hz, 2H, H_{2'ax}), 1.77 (d, *J* = 12.9 Hz, 2H, H_{3'eq}), 1.59 (dt, *J* = 8.1, 6.6 Hz, 2H, H_β), 1.39 (ddtd, *J* = 16.4, 9.5, 6.6, 3.3 Hz, 1H, H_{4'}), 1.30 (qd, *J* = 12.1, 3.8 Hz, 2H, H_{3'ax}). ¹³C NMR (126 MHz, MeOD) δ 178.24 (C₄), 165.35 (C₇), 159.75 (C₉), 157.56 (C_{8a}), 155.69 (C₂), 136.73 (C_i), 129.49 (C_o), 127.85 (C_m), 127.03 (C_p), 126.30 (C₅), 117.32 (C_{4a}), 115.30 (C₆), 110.47 (C₃), 100.34 (C₈), 62.90 (C_γ), 55.26 (C₇₁), 53.18 (C_{2'}), 37.21 (C_α), 35.49 (C_β), 33.06 (C_{4'}), 31.28 (C_{3'}). HRMS [ESI+] *m/z* = 420.2090 [M]⁺, calcd for [C₂₅H₂₈N₂O₄]⁺ 420.2049. HPLC purity 100%.

4.7.14. *N*-(2-(1-Benzylpiperidin-4-yl)ethyl)-6-nitro-4-oxo-4*H*-chromene-2-carboxamide (**14**)

Following method A, from 6-nitro-4-oxo-4*H*-chromene-2-carboxylic acid [75] (0.20 g, 0.85 mmol) and 2-(1-benzylpiperidin-4-yl)ethan-1-amine (0.23 g, 1.0 mmol), hybrid **14** was obtained (0.34 g, 92% yield) as pale-brown solid of mp 173 - 175 °C. ¹H NMR (500 MHz, MeOD) δ 8.94 (d, *J* = 2.8 Hz, 1H, H₅), 8.65 (dd, *J* = 9.2, 2.8 Hz, 1H, H₇), 7.92 (d, *J* = 9.2 Hz, 1H, H₈), 7.35 – 7.31 (m, 5H, H_{o, m}, H₃), 7.35 – 7.25 (m, 1H,

H_p), 3.55 (s, 2H, H_γ), 3.48 (dd, *J* = 8.1, 6.7 Hz, 2H, H_α), 2.94 (dt, *J* = 12.0, 3.1 Hz, 2H, H_{2'eq}), 2.07 (td, *J* = 11.9, 2.5 Hz, 2H, H_{2'ax}), 1.82 – 1.76 (m, 2H, H, H_{3'eq}), 1.61 (dt, *J* = 8.1, 6.7 Hz, 2H, H_β), 1.41 (ddt, *J* = 12.9, 6.7, 3.4 Hz, 1H, H_{4'}), 1.38 – 1.27 (m, 2H, H_{3'ax}). ¹³C NMR (126 MHz, MeOD) δ 178.83 (C₄), 160.66 (C₉), 159.84 (C₆), 157.83 (C₂), 146.65 (C_{8a}), 137.98 (C_i), 130.97 (C_o), 130.13 (C₇), 129.30 (C_m), 128.52 (C_p), 125.30 (C_{4a}), 122.57 (C₅), 121.83 (C₈), 64.28 (C_γ), 54.58 (C_{2'}), 38.71 (C_α), 36.87 (C_β), 34.44 (C_{4'}), 32.65 (C_{3'}). HRMS [ESI+] *m/z* = 435.1795 [M]⁺, calcd for [C₂₄H₂₅N₃O₅]⁺ 435.1794. HPLC purity 100%.

4.7.15. 6-Amino-*N*-(2-(1-benzylpiperidin-4-yl)ethyl)-4-oxo-4*H*-chromene-2-carboxamide (**15**)

According to method D, the amino derivative **15** (0.18 g, 98% yield) was obtained as a pale-yellow solid of mp 215 - 217 °C. ¹H NMR (400 MHz, MeOD) δ 7.50 (dd, *J* = 8.9, 0.5 Hz, 1H, H₈), 7.35 – 7.31 (m, 4H, H_{o, m}), 7.31 – 7.26 (m, 1H, H_p), 7.25 (dd, *J* = 2.9, 0.5 Hz, 1H, H₅), 7.21 (dd, *J* = 8.9, 2.9 Hz, 1H, H₇), 6.89 (s, 1H, H₃), 3.55 (s, 2H, H_γ), 3.44 (t, *J* = 7.4 Hz, 2H, H_α), 2.94 (dt, *J* = 12.1, 3.2 Hz, 2H, H_{2'eq}), 2.12 – 2.04 (m, 2H, H_{2'ax}), 1.83 – 1.75 (m, 2H, H_{3'eq}), 1.64 – 1.54 (m, 2H, H_β), 1.47 – 1.25 (m, 3H, H_{3'ax, 4'}). ¹³C NMR (101 MHz, MeOD) δ 180.68 (C₄), 161.57 (C₉), 156.84 (C₂), 150.04 (C₆), 148.37 (C_i), 131.01 (C_o), 129.32 (C_m), 128.58 (C_p), 125.92 (C_{4a}), 124.78 (C₇), 120.42 (C₈), 110.52 (C₃), 106.95 (C₅), 64.21 (C_γ), 54.57 (C_{2'}), 38.56 (C_α), 36.90 (C_β), 34.40 (C_{4'}), 32.58 (C_{3'}). HRMS [ESI+] *m/z* = 405.2063 [M]⁺, calcd for [C₂₄H₂₇N₃O₃]⁺ 405.2054. HPLC purity 100%.

4.7.16. *N*-(2-(1-Benzylpiperidin-4-yl)ethyl)-5,7-dimethoxy-4-oxo-4*H*-chromene-2-carboxamide (**16**)

Following method A, from 5,7-dimethoxy-4-oxo-4*H*-chromene-2-carboxylic acid [53] (0.15 g, 0.60 mmol) and 2-(1-benzylpiperidin-4-yl)ethan-1-amine (0.157 g, 0.72 mmol), hybrid **16** was obtained (0.24 g, 89% yield) as a white solid of mp 82 - 84 °C. ¹H NMR (300 MHz, CDCl₃) δ 7.37 – 7.21 (m, 5H, Ph), 6.95 (s, 1H, H₃), 6.83 (t, *J* = 5.9 Hz, NH), 6.48 (d, *J* = 2.3 Hz, 1H, H₈), 6.37 (d, *J* = 2.3 Hz, 1H, H₆), 3.92 (s, 3H, H₇₁), 3.88 (s, 3H, H₅₁), 3.53 – 3.44 (m, 4H, H_{α,γ}), 2.89 (d, *J* = 10.7 Hz, 2H, H_{2'eq}), 1.97 (t, *J* = 10.7 Hz, 2H, H_{2'ax}), 1.70 (d, *J* = 9.5 Hz, 2H, H_{3'eq}), 1.63 – 1.54 (m, 2H, H_β), 1.40 – 1.28 (m, 3H, H_{3'ax, 4'}). ¹³C NMR (75 MHz, CDCl₃) δ 177.05 (C₄), 164.68 (C₇), 161.29 (C₅), 159.39 (C₉), 159.05 (C_{8a}), 152.55 (C₂), 138.25 (C_i), 129.39 (C_o), 128.29 (C_m), 127.13 (C_p), 113.91 (C₃), 109.89 (C_{4a}), 96.67 (C₆), 92.94 (C₈), 63.51 (C_γ), 56.56 (C₇₁), 55.96 (C₅₁), 53.73 (C_{2'}), 37.84 (C_α), 36.29 (C_β), 33.66 (C_{4'}), 32.22 (C_{3'}). HRMS [ESI+] *m/z* = 450.2169 [M]⁺, calcd for [C₂₆H₃₀N₂O₅]⁺ 450.2155. HPLC purity 100%.

4.7.17. *N*-(2-(1-Benzylpiperidin-4-yl)ethyl)-5,7-dihydroxy-4-oxo-4*H*-chromene-2-carboxamide (**17**)

Following method C, from derivative **16** (0.05 g, 0.11 mmol) and BBr₃ (0.3 g, 1.2 mmol), hybrid **17** was obtained (0.037 g, 80%) as a pale-yellow solid of mp 267 °C (desc.) ¹H NMR (500 MHz, MeOD) δ 7.56 – 7.52 (m, 2H, H_o), 7.51 – 7.47 (m, 3H, H_{m, p}), 6.83 (s, 1H, H₃), 6.56 (d, *J* = 2.2 Hz, 1H, H₈), 6.26 (d, *J* = 2.2 Hz, 1H, H₆), 4.27 (s, 2H, H_γ), 3.48 (t, *J* = 6.9 Hz, 2H, H_α), 3.44 (d, *J* = 12.6 Hz, 2H, H_{2'eq}), 3.00 (t, *J* = 12.6 Hz, 2H, H_{2'ax}), 2.06 (d, *J* = 14.3 Hz, 2H, H_{3'eq}), 1.80 – 1.68 (m, 1H, H_{4'}), 1.65 (q, *J* = 6.9 Hz, 2H, H_β), 1.57 – 1.47 (m, 2H, H_{3'ax}). ¹³C NMR (126 MHz, MeOD) δ 183.66 (C₄),

167.08 (C₇), 163.41 (C₅), 161.04 (C₉), 158.90 (C_{8a}), 157.15 (C₂), 132.30 (C_o), 131.10 (C_i), 130.99 (C_p), 130.25 (C_m), 110.75 (C₃), 106.30 (C_{4a}), 100.75 (C₆), 95.68 (C₈), 61.68 (C_γ), 53.48 (C_{3'}), 38.06 (C_α), 36.03 (C_β), 32.33 (C_{4'}), 30.24 (C_{3'}). HRMS [ESI+] *m/z* =422.1852 [M]⁺, calcd for [C₂₄H₂₆N₂O₅]⁺ 422.1842. HPLC purity 98%.

4.7.18. *N*-(2-(1-Benzylpiperidin-4-yl)ethyl)-6,7-dimethoxy-4-oxo-4*H*-chromene-2-carboxamide (**18**)

Following method B, from 6,7-dimethoxy-4-oxo-4*H*-chromene-2-carboxylic acid [53] (0.2 g, 0.80 mmol) and 2-(1-benzylpiperidin-4-yl)ethan-1-amine (0.191 g, 0.88 mmol), hybrid **18** was obtained (0.28 g, 80% yield) as a white solid of mp 129 - 131 °C. ¹H NMR (300 MHz, CDCl₃) δ 7.46 (s, 1H, H₅), 7.32 – 7.18 (m, 5H, Ph), 7.05 (s, 1H, H₈), 6.90 (s, 2H, NH, H₃), 3.94 (s, 3H, H₇₁), 3.92 (s, 3H, H₆₁), 3.53 – 3.38 (m, 4H, H_{α, γ}), 2.88 (dd, *J* = 11.5, 3.9 Hz, 2H, H_{2'eq}), 1.97 (t, *J* = 11.5 Hz, 2H, H_{2'ax}), 1.75 – 1.63 (m, 2H, H_{3'eq}), 1.63 – 1.44 (m, 2H, H_β), 1.39 – 1.22 (m, 3H, H_{3'ax, 4'}). ¹³C NMR (75 MHz, CDCl₃) δ 177.30 (C₄), 159.42 (C₉), 155.19 (C₇), 154.37 (C_{8a}), 151.39 (C₂), 148.29 (C₆), 137.73 (C_i), 129.46 (C_o), 128.31 (C_m), 127.26 (C_p), 117.97 (C_{4a}), 111.61 (C₈), 104.51 (C₅), 99.77 (C₃), 63.34 (C_γ), 56.67 (C₆₁), 56.49 (C₇₁), 53.60 (C_{2'}), 37.85 (C_α), 36.20 (C_β), 33.51 (C_{4'}), 32.02 (C_{3'}). HRMS [ESI+] *m/z* =450.2176 [M]⁺, calcd for [C₂₆H₃₀N₂O₅]⁺ 450.2155. HPLC purity 100%.

4.7.19. *N*-(2-(1-Benzylpiperidin-4-yl)ethyl)-6,7-dihydroxy-4-oxo-4*H*-chromene-2-carboxamide (**19**)

Following method C, from compound **18** (0.05 g, 0.12 mmol) and BBr₃ (0.3 g, 1.2 mmol), hybrid **19** was obtained (0.04 g, 85% yield) as a pale-yellow solid of mp 204 °C

(desc.) ^1H NMR (300 MHz, MeOD) δ 7.54 – 7.46 (m, 2H, H_o), 7.45 – 7.39 (m, 3H, H_m , H_p), 7.32 (s, 1H, H_8), 7.03 (s, 1H, H_5), 6.81 (s, 1H, H_3), 4.21 (s, 2H, H_γ), 3.48 – 3.34 (m, 4H, $\text{H}_{2'_{\text{eq}}, \alpha}$), 2.93 (td, $J = 12.5, 2.8$ Hz, 2H, $\text{H}_{2'_{\text{ax}}}$), 2.00 (d, $J = 13.8$ Hz, 2H, $\text{H}_{3'_{\text{eq}}}$), 1.71 – 1.38 (m, 5H, $\text{H}_{3'_{\text{ax}}, \beta, 4'}$). ^{13}C NMR (75 MHz, MeOD) δ 179.57 (C_4), 161.58 (C_9), 156.33 (C_2), 155.69 (C_7), 152.96 (C_6), 146.97 (C_{8a}), 132.34 (C_o), 131.04 (C_p), 130.80 (C_i), 130.24 (C_m), 117.87 (C_{4a}), 110.85 (C_3), 108.13 (C_8), 104.19 (C_5), 61.55 (C_γ), 53.41 ($\text{C}_{2'}$), 38.02 (C_α), 35.98 (C_β), 32.22 ($\text{C}_{4'}$), 30.12 (C_3). HRMS [ESI+] $m/z = 422.1852$ [M] $^+$, calcd for $[\text{C}_{24}\text{H}_{26}\text{N}_2\text{O}_5]^+$ 422.1842. HPLC purity 97%.

4.7.20. *N*-(3-(1-Benzylpiperidin-4-yl)propyl)-6-methoxy-4-oxo-4H-chromene-2-carboxamide (**20**)

Following method B, from 6-methoxy-4-oxo-4H-chromene-2-carboxylic acid [53] (0.25 g, 1.11 mmol) and 3-(1-benzylpiperidin-4-yl)propan-1-amine (0.29 g, 1.25 mmol), hybrid **20** was obtained (0.28 g, 59% yield) as a light-yellow solid of mp 149 - 151 °C. ^1H NMR (500 MHz, MeOD) δ 7.67 (d, $J = 9.3$ Hz, 1H, H_8), 7.53 (d, $J = 3.1$ Hz, 1H, H_5), 7.45 (dd, $J = 9.3, 3.1$ Hz, 1H, H_7), 7.35 – 7.30 (m, 4H, H_o, m), 7.30 – 7.25 (m, 1H, H_p), 6.96 (s, 1H, H_3), 3.91 (s, 3H, H_{61}), 3.56 (s, 2H, H_γ), 3.40 (t, $J = 7.4$ Hz, 2H, H_α), 2.94 (dt, $J = 12.0, 3.3$ Hz, 2H, $\text{H}_{2'_{\text{eq}}}$), 2.08 (td, $J = 12.0, 11.4, 2.5$ Hz, 2H, $\text{H}_{2'_{\text{ax}}}$), 1.74 (d, $J = 13.1$ Hz, 2H, $\text{H}_{3'_{\text{eq}}}$), 1.67 (p, $J = 7.4$ Hz, 2H, H_β), 1.37 – 1.25 (m, 5H, $\text{H}_{3'_{\text{ax}}, 4', \delta}$). ^{13}C NMR (126 MHz, MeOD) δ 180.23 (C_4), 161.29 (C_9), 159.21 (C_6), 157.26 (C_2), 151.82 (C_{8a}), 137.68 (C_i), 131.03 (C_o), 129.32 (C_m), 128.61 (C_p), 125.90 (C_7), 125.79 (C_{4a}), 121.30 (C_8), 110.98 (C_3), 105.68 (C_5), 64.19 (C_γ), 56.42 (C_{61}), 54.65 ($\text{C}_{2'}$), 41.15 (C_α), 36.38 ($\text{C}_{4'}$), 34.72 (C_δ), 32.69 ($\text{C}_{3'}$), 27.52 (C_β). HRMS [ESI+] $m/z = 434.2214$ [M] $^+$, calcd for $[\text{C}_{26}\text{H}_{30}\text{N}_2\text{O}_4]^+$ 434.2206. HPLC purity 100%.

4.7.21. *N*-(3-(1-Benzylpiperidin-4-yl)propyl)-6-hydroxy-4-oxo-4*H*-chromene-2-carboxamide (**21**)

Following method C, from compound **20** (0.05 g, 0.09 mmol) and BBr₃ (0.3 g, 1.2 mmol), hybrid **21** was obtained (0.043 g, 90% yield) as a pale-brown solid of mp 208 - 210 °C. ¹H NMR (500 MHz, MeOD) δ 7.65 (d, *J* = 9.1 Hz, 1H, H₈), 7.56 – 7.52 (m, 2H, H_o), 7.49 – 7.47 (m, 3H, H_{m, p}), 7.41 (d, *J* = 3.0 Hz, 1H, H₅), 7.33 (dd, *J* = 9.1, 3.0 Hz, 1H, H₇), 6.92 (s, 1H, H₃), 4.30 (s, 2H, H_γ), 3.47 – 3.40 (m, 4H, H_{2'eq, α}), 3.02 (td, *J* = 12.8, 3.1 Hz, 2H, H_{2'ax}), 2.02 – 1.97 (m, 2H, H_{3'eq}), 1.73 – 1.65 (m, 3H, H_{4', β}), 1.54 – 1.44 (m, 2H, H_{3'ax}), 1.43 – 1.36 (m, 2H, H_δ). ¹³C NMR (126 MHz, MeOD) δ 180.44 (C₄), 161.47 (C₉), 157.18 (C_{8a}), 157.13 (C₂), 150.97 (C₆), 132.36 (C_o), 131.11 (C_p), 130.72 (C_i), 130.29 (C_m), 125.95 (C_{4a}), 125.54 (C₇), 121.19 (C₈), 110.69 (C₃), 108.71 (C₅), 61.57 (C_γ), 53.54 (C_{2'}), 40.81 (C_α), 34.32 (C_{4'}), 33.66 (C_δ), 30.33 (C_{3'}), 27.30 (C_β). HRMS [ESI+] *m/z* = 420.2045 M]⁺, calcd for [C₂₅H₂₈N₂O₄]⁺ 420.2049. HPLC purity 99%.

4.7.22. *N*-(3-(1-Benzylpiperidin-4-yl)propyl)-6,7-dimethoxy-4-oxo-4*H*-chromene-2-carboxamide (**22**)

Following method B, from 6,7-dimethoxy-4-oxo-4*H*-chromene-2-carboxylic acid [53] (0.21 g, 1.0 mmol) and 3-(1-benzylpiperidin-4-yl)propan-1-amine (0.22 g, 1.1 mmol), hybrid **22** was obtained (0.23 g, 60% yield) as a light-yellow solid of mp 99 - 102 °C. ¹H NMR (500 MHz, MeOD) δ 7.46 (s, 1H, H₅), 7.35 – 7.31 (m, 4H, H_{o, m}), 7.30 – 7.26 (m, 1H, H_p), 7.20 (s, 1H, H₈), 6.92 (s, 1H, H₃), 3.99 (s, 3H, H₆₁), 3.93 (s, 3H, H₇₁), 3.58 (s, 2H, H_γ), 3.40 (t, *J* = 7.2 Hz, 2H, H_α), 2.95 (dt, *J* = 12.2, 3.1 Hz, 2H, H_{2'eq}),

2.10 (td, $J = 12.2, 11.5, 2.5$ Hz, 2H, $H_{2'ax}$), 1.75 (d, $J = 12.8$ Hz, 2H, $H_{3'eq}$), 1.67 (p, $J = 7.7$ Hz, 2H, H_{β}), 1.39 – 1.32 (m, 3H, $H_{\delta, 4'}$), 1.31 – 1.23 (m, 2H, $H_{3'ax}$). ^{13}C NMR (126 MHz, MeOD) δ 179.46 (C_4), 161.29 (C_9), 157.38 (C_6), 156.80 (C_2), 153.42 (C_{8a}), 150.04 (C_7), 137.50 (C_i), 131.06 (C_o), 129.35 (C_m), 128.68 (C_p), 118.37 (C_{4a}), 111.29 (C_3), 104.70 (C_5), 101.21 (C_8), 64.12 (C_γ), 57.07 (C_{61}), 56.67 (C_{71}), 54.63 ($C_{2'}$), 41.12 (C_α), 36.35 ($C_{4'}$), 34.70 (C_δ), 32.64 ($C_{3'}$), 27.53 (C_β). HRMS [ESI+] $m/z = 464.2304$ $[\text{M}]^+$, calcd for $[\text{C}_{27}\text{H}_{32}\text{N}_2\text{O}_5]^+$ 464.2311. HPLC purity 100%.

4.7.23. *N*-(2-(1-Benzylpiperidin-4-yl)ethyl)-6-methoxy-4-oxo-1,4-dihydroquinoline-2-carboxamide (**23**)

Following method E, from methyl 6-methoxy-4-oxo-1,4-dihydroquinoline-2-carboxylate [76] (0.1 g, 0.43 mmol) and 2-(1-benzylpiperidin-4-yl)ethan-1-amine (0.23 g, 1.07 mmol), hybrid **23** was obtained (0.143g, 80% yield) as a white solid of mp 184 - 186 °C. ^1H NMR (300 MHz, MeOD) δ 8.16 (d, $J = 9.3$ Hz, 1H, H_8), 7.75 – 7.41 (m, 8H, Ph, $H_{3, 7, 5}$), 4.30 (s, 2H, H_γ), 3.99 (s, 3H, H_{61}), 3.62 – 3.38 (m, 4H, $H_{\alpha, 2'eq}$), 3.04 (t, $J = 13.0$ Hz, 2H, $H_{2'ax}$), 2.07 (d, $J = 14.2$ Hz, 2H, $H_{3'eq}$), 1.93 – 1.61 (m, 3H, $H_{\beta, 4'}$), 1.61 – 1.42 (m, 2H, $H_{3'ax}$). ^{13}C NMR (75 MHz, MeOD) δ 171.74 (C_4), 161.25 (C_9), 160.95 (C_6), 144.92 (C_2), 136.53 (C_{8a}), 132.47 (C_o), 131.19 (C_p), 130.42 (C_i), 130.30 (C_m), 129.05 (C_7), 124.45 (C_{4a}), 123.40 (C_8), 104.38 (C_3), 102.42 (C_5), 61.78 (C_γ), 56.69 (C_{61}), 53.71 ($C_{2'}$), 38.63 (C_α), 35.95 (C_β), 32.35 ($C_{4'}$), 30.35 ($C_{3'}$). HRMS [ESI+] $m/z = 419.2203$ $[\text{M}]^+$, calcd for $[\text{C}_{25}\text{H}_{29}\text{N}_3\text{O}_3]^+$ 419.2209. HPLC purity 100%.

4.7.24. *N*-(2-(1-Benzylpiperidin-4-yl)ethyl)-6-hydroxy-4-oxo-1,4-dihydroquinoline-2-carboxamide (**24**)

Following method C, from derivative **23** (0.03 g, 0.07 mmol) and BBr₃ (0.13 g, 0.5 mmol), hybrid **24** was obtained (0.02 g, 70% yield) as a white solid of mp 167 – 169 °C. ¹H NMR (500 MHz, DMSO-*d*₆) δ 11.71 (s, 1H, NH₁), 9.77 (s, 1H, OH), 8.93 (t, *J* = 5.7 Hz, 1H, NH₁₀), 7.82 (d, *J* = 8.7 Hz, 1H, H₈), 7.56 – 7.42 (m, 5H, Ph), 7.36 (d, *J* = 2.9 Hz, 1H, H₅), 7.18 (dd, *J* = 8.7, 2.9 Hz, 1H, H₇), 6.59 (s, 1H, H₃), 4.28 (s, 2H, H₇), 3.33 (s, 4H, H_{α, 2'eq}), 2.98 – 2.84 (m, 2H, H_{2'ax}), 1.97 – 1.87 (m, 2H, H_{3'eq}), 1.63 – 1.45 (m, 3H, H_{β, 4'}), 1.44 – 1.34 (m, 2H, H_{3'ax}). ¹³C NMR (126 MHz, DMSO-*d*₆) δ 177.38 (C₄), 162.40 (C₉), 154.51 (C₆), 140.61 (C₂), 133.75 (C_{8a}), 131.82 (C_o), 129.99 (C_i), 129.37 (C_p), 129.26 (C_m), 127.56 (C_{4a}), 123.12 (C₇), 121.57 (C₈), 107.32 (C₅), 105.44 (C₃), 59.60 (C_γ), 52.01 (C_{2'}), 37.02 (C_α), 35.09 (C_β), 30.87 (C_{4'}), 29.06 (C_{3'}). HRMS [ESI+] *m/z* = 405.2059 [M]⁺, calcd for [C₂₄H₂₇N₃O₃]⁺ 405.2052. HPLC purity 100%.

4.7.25. *N*-(2-(1-Benzylpiperidin-4-yl)ethyl)-7-methoxy-4-oxo-1,4-dihydroquinoline-2-carboxamide (**25**)

Following method E, from methyl 7-methoxy-4-oxo-1,4-dihydroquinoline-2-carboxylate [77] (0.1 g, 0.43 mmol) and 2-(1-benzylpiperidin-4-yl)ethan-1-amine (0.23 g, 1.07 mmol), hybrid **25** was obtained (0.12 g, 65% yield) as a white solid of mp 201 – 203 °C. ¹H NMR (300 MHz, MeOD) δ 8.27 (d, *J* = 9.4 Hz, 1H, H₅), 7.69 – 7.39 (m, 7H, Ph, H_{3, 8}), 7.37 (dd, *J* = 9.4, 2.3 Hz, 1H, H₆), 4.30 (s, 2H, H₇), 4.02 (s, 3H, H₇₁), 3.58 – 3.41 (m, 4H, H_{α, 2'eq}), 3.05 (t, *J* = 12.5 Hz, 2H, H_{2'ax}), 2.06 (d, *J* = 14.2 Hz, 2H, H_{3'eq}), 1.80 – 1.44 (m, 5H, H_{β, 4', 3'ax}). ¹³C NMR (75 MHz, MeOD) δ 172.32 (C₄), 167.01 (C₇), 160.96 (C₉), 146.61 (C₂), 143.66 (C_{8a}), 132.49 (C_o), 131.14 (C_p), 130.45 (C_i), 130.26

(C_m), 126.58 (C₅), 122.17 (C₆), 117.00 (C_{4a}), 103.81 (C₃), 100.32 (C₈), 61.73 (C_γ), 57.04 (C₇₁), 53.68 (C_{2'}), 38.64 (C_α), 35.88 (C_β), 32.29 (C_{4'}), 30.32 (C_{3'}). HRMS [ESI+] *m/z* =419.2212 [M]⁺, calcd for [C₂₅H₂₉N₃O₃]⁺ 419.2209. HPLC purity 100%.

4.7.26. *N*-(2-(1-Benzylpiperidin-4-yl)ethyl)-8-methoxy-4-oxo-1,4-dihydroquinoline-2-carboxamide (**26**)

Following method E, from methyl 8-methoxy-4-oxo-1,4-dihydroquinoline-2-carboxylate [78] (0.1 g, 0.43 mmol) and 2-(1-benzylpiperidin-4-yl)ethan-1-amine (0.23 g, 1.07 mmol), hybrid **26** was obtained (0.11 g, 60% yield) as a white solid of mp 187 - 189 °C. ¹H NMR (500 MHz, MeOD) δ 7.80 (bs, 1H, CH), 7.56 – 7.49 (m, 6H, CH, Ph), 7.41 (bs, 1H, CH), 7.37 – 7.32 (m, 1H, CH), 6.89 (bs, 1H, NH), 4.30 (s, 2H, H_γ), 4.11 (s, 3H, H₈₁), 3.54 – 3.49 (m, 4H, H_{α, 2'eq}), 3.06 – 2.98 (m, 2H, H_{2'ax}), 2.09 (d, *J* = 13.7 Hz, 2H, H_{3'eq}), 1.78 – 1.62 (m, 3H, H_{4',β}), 1.59 – 1.45 (m, 2H, H_{3'ax}). ¹³C NMR (126 MHz, MeOD) δ 172.97 (C₄), 163.29 (C₉), 150.74 (C₈), 132.47 (C_o), 132.05 (C), 131.26 (C_p), 130.50 (C), 130.37 (C_i), 130.36 (C_m), 126.28 (CH), 116.99 (CH), 112.78 (CH), 61.95 (C_γ), 57.10 (C₈₁), 53.88 (C_{2'}), 38.38 (C_α), 36.16 (C_β), 32.44 (C_{4'}), 30.43 (C_{3'}). HRMS [ESI+] *m/z* =419.2207 [M]⁺, calcd for [C₂₅H₂₉N₃O₃]⁺ 419.2209. HPLC purity 100%.

4.7.27. *N*-(2-(1-Benzylpiperidin-4-yl)ethyl)-8-hydroxy-4-oxo-1,4-dihydroquinoline-2-carboxamide (**27**)

Following method C, from derivative **26** (70 mg, 0.17 mmol) and BBr₃ (0.29 g, 1.17 mmol), hybrid **27** was obtained (61 mg, 90% yield) as a white solid of mp 185 - 187 °C. ¹H NMR (500 MHz, MeOD) δ 7.72 (dd, *J* = 8.4, 1.2 Hz, 1H, H₅), 7.57 – 7.46

(m, 6H, Ph, H₃), 7.41 (dd, $J = 8.4, 7.6$ Hz, 1H, H₆), 7.24 (bs, 1H, NH), 7.19 (dd, $J = 7.6, 1.2$ Hz, 1H, H₇), 4.30 (s, 2H, H_γ), 3.54 (t, $J = 6.8$ Hz, 2H, H_α), 3.52 – 3.48 (m, 2H, H_{2'eq}), 3.08 – 2.99 (m, 2H, H_{2'ax}), 2.11 (d, $J = 14.5$ Hz, 2H, H_{3'eq}), 1.80 – 1.71 (m, 1H, H_{4'}), 1.68 (q, $J = 6.8$ Hz, 2H, H_β), 1.54 – 1.43 (m, 2H, H_{3'ax}). ¹³C NMR (126 MHz, MeOD) δ 164.66 (C₉), 132.38 (C_o), 131.29 (C_p), 130.37 (C_m), 127.84 (C₆), 114.76 (CH), 61.87 (C_γ), 53.77 (C_{2'}), 38.08 (C_α), 36.29 (C_β), 32.37 (C_{4'}), 30.45 (C_{3'}). HRMS [ESI+] $m/z = 405.2053$ [M]⁺, calcd for [C₂₄H₂₇N₃O₃]⁺ 405.2052. HPLC purity 99%.

4.7.28. *N*-(2-(1-Benzylpiperidin-4-yl)ethyl)-6,7-dimethoxy-4-oxo-1,4-dihydroquinoline-2-carboxamide (**28**)

Following method E, from methyl 6,7-dimethoxy-4-oxo-1,4-dihydroquinoline-2-carboxylate [79] (0.12 g, 0.40 mmol) and 2-(1-benzylpiperidin-4-yl)ethan-1-amine (0.22 g, 0.9 mmol), hybrid **28** was obtained (0.1 g, 50% yield) as a white solid of mp 255 – 256 °C. ¹H NMR (500 MHz, MeOD) δ 7.59 (s, 1H, H₈), 7.54 – 7.50 (m, 2H, H_o), 7.47 – 7.43 (m, 3H, H_{m,p}), 7.35 (s, 1H, H₅), 6.81 (s, 1H, H₅), 4.16 (s, 2H, H_γ), 4.00 (s, 3H, H₇₁), 3.96 (s, 3H, H₆₁), 3.50 (t, $J = 6.7$ Hz, 2H, H₁₅), 3.39 – 3.33 (m, 2H, H_{2'eq}), 2.85 (t, $J = 12.6$ Hz, 2H, H_{2'ax}), 2.01 (d, $J = 13.2$ Hz, 2H, H_{3'eq}), 1.70 – 1.63 (m, 3H, H_{β, 4'}), 1.60 – 1.48 (m, 2H, H_{3'ax}). ¹³C NMR (126 MHz, MeOD) δ 163.85 (C₉), 156.23 (C₇), 150.05 (C₆), 142.81 (C₂), 138.37 (C_{8a}), 132.11 (C_o), 130.56 (C_p), 130.07 (C_m), 120.88 (C_{4a}), 106.42 (C₃), 104.27 (C₈), 101.21 (C₆), 62.03 (C₂₃), 56.78 (C₇₁), 56.50 (C₆₁), 53.64 (C_{2'}), 38.38 (C_α), 36.14 (C_β), 32.74 (C_{4'}), 30.60 (C_{3'}). C_{4a}, C₂ Ci not observed. HRMS [ESI+] $m/z = 449.2315$ [M]⁺, calcd for [C₂₆H₃₁N₃O₄]⁺ 449.2315. HPLC purity 100%.

4.7.29. *N*-(2-(1-Benzylpiperidin-4-yl)ethyl)-4,6,7-trimethoxyquinoline-2-carboxamide
(29)

Following method E, from methyl 4,6,7-trimethoxyquinoline-2-carboxylate (0.05 g, 0.18 mmol) and 2-(1-benzylpiperidin-4-yl)ethan-1-amine (0.059 g, 0.27 mmol), hybrid **29** was obtained (54 mg, 65% yield) as a white solid of mp 182 - 184 °C. ¹H NMR (500 MHz, CDCl₃) δ 8.45 (s, 1H, H₈), 8.07 (s, 1H, H₃), 7.67 – 7.56 (m, 2H, H_m), 7.44 (s, 1H, H₅), 7.40 – 7.33 (m, 3H, H_{o, p}), 4.35 (s, 3H, H₄₁), 4.11 (s, 5H, H_{71, γ}), 4.05 (s, 3H, H₆₁), 3.66 – 3.52 (m, 2H, H_α), 3.51 – 3.38 (m, 2H, H_{2'eq}), 2.90 – 2.62 (m, 2H, H_{2'ax}), 2.06 – 1.92 (m, 5H, H_{4', 3'}), 1.78 – 1.60 (m, 2H, H_β). ¹³C NMR (126 MHz, CDCl₃) δ 167.05 (C₄), 158.28 (C₉), 157.03 (C₇), 152.21 (C₆), 143.69 (C₂), 137.12 (C_{8a}), 131.62 (C_m), 130.03 (C_p), 129.25 (C_o), 128.48 (C_i), 116.90 (C_{4a}), 101.10 (C₃), 100.97 (C₈), 100.09 (C₅), 61.15 (C_γ), 58.62 (C₄₁), 57.35 (C₇₁), 56.72 (C₆₁), 52.79 (C_{2'}), 37.67 (C_α), 34.32 (C_β), 30.98 (C_{4'}), 28.80 (C_{3'}). HRMS [ESI+] *m/z* =463.24746 [M]⁺, calcd for [C₂₇H₃₃N₃O₄]⁺ 463.24711. HPLC purity 100%.

4.8. Biochemical studies

4.8.1. Inhibition of human cholinesterases

Using human recombinant acetylcholinesterase (h-AChE) and butyrylcholinesterase from human serum (h-BuChE), the Ellman method was followed [50], according to the experimental details previously described [37].

4.8.2. *In vitro* blood–brain barrier permeation assay (PAMPA-BBB)

Prediction of the brain penetration was evaluated using a parallel artificial membrane permeation assay (PAMPA-BBB), in a similar manner as previously described [37,52-54]. Pipetting was performed with a semi-automatic pipettor (CyBi®-SELMA) and UV reading with a microplate spectrophotometer (Multiskan Spectrum, Thermo Electron Co.). Commercial drugs, phosphate buffered saline solution at pH 7.4 (PBS), and dodecane were purchased from Sigma, Aldrich, Acros, and Fluka. Millex filter units (PVDF membrane, diameter 25 mm, pore size 0.45 μm) were acquired from Millipore. The porcine brain lipid (PBL) was obtained from Avanti Polar Lipids. The donor microplate was a 96-well filter plate (PVDF membrane, pore size 0.45 μm) and the acceptor microplate was an indented 96-well plate, both from Millipore. The acceptor 96-well microplate was filled with 200 μL of PBS : ethanol (70:30) and the filter surface of the donor microplate was impregnated with 5 μL of porcine brain lipid (PBL) in dodecane (20 mg mL^{-1}). Compounds were dissolved in PBS:ethanol (70:30) at 100 $\mu\text{g mL}^{-1}$, filtered through a Millex filter, and then added to the donor wells (200 μL). The donor filter plate was carefully put on the acceptor plate to form a sandwich, which was left undisturbed for 120 min at 25 $^{\circ}\text{C}$. After incubation, the donor plate is carefully removed and the concentration of compounds in the acceptor wells was determined by UV-Vis spectroscopy. Every sample is analyzed at five wavelengths, in four wells and at least in three independent runs, and the results are given as the mean \pm standard deviation. In each experiment, 11 quality control standards of known BBB permeability were included to validate and normalize the analysis set.

4.8.3. Inhibition of human 5-lipoxygenase (5-LOX)

The fluorescence-based enzyme method developed by Pufahl et al. was followed [55], in 96-well microtiter plates. The assay solution consists of Tris buffer (50 mM, pH 7.5), ethylenediaminetetraacetic acid (EDTA, 2 mM), CaCl_2 (2 mM), arachidonic acid (AA, 3 μM), ATP (10 μM), 2',7'-dichlorodihydrofluorescein diacetate (H_2DCFDA , 10 μM), 5-lipoxygenase (100 mU/well), bovine glutathione peroxidase (GPx, 25 mU/well) and reduced glutathione (GSH, 1 mM). Compounds to be tested were added to the test solution prior to AA and ATP, and preincubated for a period of 10 minutes at room temperature. Then, the AA and ATP substrates were added; the enzymatic reaction allowed to progress for 20 minutes and ended by the addition of 40 μL of acetonitrile. The fluorescence measurements (excitation: 485 nm; emission: 520 nm) were performed on a FLUOstar OPTIMA (BMG LABTECH, Offenburg, Germany). IC_{50} is defined as the concentration of compound that inhibits enzymatic activity by 50% over the control of untreated enzyme.

4.8.4. Inhibition of human monoamine oxidases

MAO inhibition measurements were evaluated following the general procedure previously described by a part of us [80]. Briefly, test drugs and adequate amounts of recombinant hMAO-A or hMAO-B (Sigma-Aldrich Química S.A., Alcobendas, Spain) required and adjusted to oxidize 165 pmol of p-tyramine/min in the control group, were incubated for 15 min at 37 °C in a flat-black-bottom 96-well microtest plate (BD Biosciences, Franklin Lakes, NJ) placed in the dark fluorimeter chamber. The reaction was started by adding 200 mM Amplex Red reagent (Molecular Probes, Inc., Eugene, OR), 1 U/mL horseradish peroxidase, and 1 mM p-tyramine and the production of

resorufin, was quantified at 37 °C in a multidetection microplate fluorescence reader (FLX800, Bio-Tek Instruments, Inc., Winooski, VT) based on the fluorescence generated (excitation, 545 nm; emission, 590 nm). The specific fluorescence emission was calculated after subtraction of the background activity, which was determined from wells containing all components except the hMAO isoforms, which were replaced by a sodium phosphate buffer solution.

4.8.5. Oxygen radical absorbance capacity assay (ORAC)

The ORAC method was followed, using a Polarstar Galaxy plate reader (BMG Labtechnologies GmbH, Offenburg, Germany) with 485-P excitation and 520-P emission filters [81].

4.8.6. Binding assays at sigma-1 and sigma-2 receptors

For σ_1 R assay, the thawed membrane preparation of guinea pig brain cortex (about 100 μ g of protein) were incubated for 120 min at 37°C with 2 nM [3 H]-(+)-pentazocine (PerkinElmer, specific activity 34.9 Ci/mmol) in 50 mM Tris-HCl, pH 7.4, 0.5 mL final volume. Nonspecific binding was defined in the presence of 10 μ M of unlabeled (+)-pentazocine. The reaction was stopped by vacuum filtration through GF/B glass-fiber filters presoaked with 0.5% polyethylenimine, followed by rapid washing with 2 ml ice-cold buffer. Filters were placed in 3 ml scintillation cocktail and the radioactivity determined by liquid scintillation counting.

For σ_2 R assay, 150 μ g of rat liver homogenate were incubated for 120 min at room temperature with 3 nM [3 H]-DTG (PerkinElmer, specific activity 58.1 Ci/mmol) in 50

mM Tris-HCl, pH 8.0, 0.5 mL final volume. (+)-Pentazocine (500 nM) was used to mask σ_1R and to define nonspecific binding, respectively.

Competition studies were done using at least 11 different concentrations of the ligand under investigation. As control, three increasing concentrations of unlabelled (+)-pentazocine (σ_1R) or DTG (σ_2R) were always included. The compounds were prepared as 10 mM stock solutions in 100% DMSO and diluted with Tris-HCl buffer on the day of the experiment. The final DMSO concentration in the incubation tubes was maintained at 0.1% [57].

IC₅₀ values and Hill's coefficients n_H were calculated by nonlinear regression using a four parameters curve-fitting algorithm of the GraphPad Prism software (v.6, La Jolla California USA), and are reported as the mean \pm SEM of three separate determinations performed in duplicate. The corresponding K_i values were obtained by means of the Cheng-Prusoff equation, using the K_d values obtained in saturation experiments.

4.8.7. Study of theoretical medicinal chemistry alerts in free databases

SMILES code of hybrids **1-29** were uploaded in two databases, namely ZINC15 (<http://zinc15.docking.org/>) [58] and SwissADME (<http://www.swissadme.ch/>) [59]. PAINs and aggregation results are gathered in Table S1 (Supplementary information).

4.8.8. Neuroprotection studies

Human neuroblastoma SH-SY5Y cells were maintained in a 1:1 mixture of nutrient mixture F-12 and Eagle's minimum essential medium (EMEM) supplemented with 15 nonessential amino acids, sodium pyruvate (1 mM), 10% heat-inactivated FBS, 100 units/ml penicillin, and 100 μ g/ml streptomycin. Cultures were seeded into flasks

containing supplemented medium and maintained at 37 °C in a humidified atmosphere of 5% CO₂ and 95% air. For assays, SH-SY5Y cells were subcultured in 96-well plates at a seeding density of 8x10⁴ cells per well for 2 days. Cells were co-incubated with tested compounds (at concentrations of 0.1, 0.3, 1 and 3 μM) and the mixture rotenone (30 μM) / oligomycin A (10 μM) (R/O) for 24h in F-12/EMEM with 1% FBS. A vehicle group containing 0.1% dimethyl sulfoxide (DMSO) was employed in parallel for each experiment, and melatonin and donepezil were used as reference drugs. All SH-SY5Y cells used in this study were used at a low passage number (<13).

The measurement of cell viability was performed by the MTT reduction assay, as previously described [82]. Briefly, 50 μL of the MTT labelling reagent, at a final concentration of 0.5 mg/mL, was added. After incubation for 2 h, in a humidified incubator at 37 °C with 5% CO₂ and 95% air (v/v), the supernatant was removed, the obtained purple formazan product was re-suspended in 100 μL of dimethyl sulfoxide (DMSO). Colorimetric determination of MTT reduction was measured in an ELISA microplate reader at 540 nm. Control cells treated with EMEM were taken as 100% viability.

4.8.9. Neurogenic assays

Adult (3 months old) male C57BL/6 mice were used following the animal experimental procedures previously approved by the Ethics Committee for Animal Experimentation of the CSIC in accordance with the European Communities Council, directive 2010/63/EEC and National regulations, normative 53/2013. Special care was taken to minimize animal suffering. Neural stem cells were isolated from the SGZ of the dentate gyrus of the hippocampus of adult mice and cultured as NS according to previously published protocols [65,66]. Neural stem cells grown as NS were treated for

7 days in culture with compound **18** (10 μ M). Now, NS were adhered onto 100 μ g/mL poly-L-lysine-coated coverslips and treated for 3 additional days in the presence of serum but in the absence of exogenous growth factors to induce differentiation [67]. Finally, the expression of neuronal markers was analyzed by immunocytochemistry using antibodies linked to neurogenesis: β -III-tubulin polyclonal antibody (TuJ clone; Abcam), a protein expressed at early stages of neurogenesis and a monoclonal microtubule-associated protein type 2 (MAP-2) antibody, a classical marker of late neuronal maturation. To visualize primary antibodies Alexa-fluor-labeled secondary antibodies (Molecular probes) were used. Nuclei were stained with DAPI. Finally, images were acquired in a LSM710 laser scanning spectral confocal microscope (Zeiss). Confocal microscope settings were adjusted to produce the optimum signal-to-noise ratio.

4.8.10. *In silico* toxicity and metabolism predictions

To assess toxicity prediction, we use Derek Nexus v 6.0.1 (knowledge base 2018 1.1, species: human), which is a knowledge-based expert system by Lhasa Limited where toxicity predictions consider the presence of a toxicophore in the query structure and are the result of two processes: evaluating alerts and estimating the likelihood of toxicity [68]. The likelihood levels in Derek Nexus in highest to lowest order are: certain, probable, plausible, equivocal, doubted, improbable, and impossible [69].

To predict metabolism, we use Meteor Nexus v 3.1.0 (knowledge base 2018 1.0.0), which is a knowledge-based approach to rank metabolites based on known metabolic reactions [68]. To predict first metabolic step of the parent compound (hybrid **18**), we analyze the phase-I biotransformation pathways. An absolute reasoning was applied to evaluate the likelihood level for a biotransformation to occur, and the minimal

likelihood level was settled in “plausible”, what means that the weight of evidence supports the proposition [69].

4.8.11. Computational binding studies

All simulations were carried out using the Pmemd modules of Amber 16 [83], running on our own CPU/GPU calculation cluster. Molecular graphics images were produced using the UCSF Chimera package (v.1.10) [84]. Chimera is developed by the Resource for Biocomputing, Visualization, and Informatics at the University of California, San Francisco (supported by NIGMS P41-GM103311). All other graphs were obtained using GraphPad Prism (v. 6.0). The molecular structures of hAChE and of 5-LOX were obtained from the Protein Data Bank (pdb code: 4EY7 [72] and pdb code: 3V99 [85], respectively) while the optimized membrane-bound 3D structure of the σ 1 receptor was obtained starting from the available Protein Data Bank file (pdb code: 5HK1) [86] and following a procedure previously described [87,88].

The optimized structure of **18** was docked into each protein identified binding pocket using Autodock 4.2.6/Autodock Tools 1.4.6 [70] on a win64 platform. The resulting docked conformations were clustered and visualized; then, the structure of each resulting complex characterized by the lowest Autodock interaction energy in the prevailing cluster was selected for further modeling. Each compound/protein complex obtained from the docking procedure was further refined in Amber 16 using the quenched molecular dynamics (QMD) method as previously described [see, for example, Refs. [35,89-91] and references therein]. Next, the best energy configuration of each complex resulting from QMD was subsequently solvated by a cubic box of TIP3P water molecules, extending at least 10 Å in each direction from the solute [92]. The system was neutralized and the solution ionic strength was adjusted to the

physiological value of 0.15 M by adding the proper amounts of Na⁺ and Cl⁻ ions. Each solvated system was relaxed (500 steps of steepest descent followed by 500 other conjugate-gradient minimization steps) and then gradually heated to the target temperature of 298 K in intervals of 50 ps of constant volume-constant temperature (NVT) molecular dynamics (MD) simulations (Verlet integration method, time step 1.0 fs). The Langevin thermostat was used to control temperature. During this phase of MD, the protein was restrained with a force constant of 2.0 kcal/(mol Å), and all simulations were carried out with periodic boundary conditions. Subsequently, the density of the system was equilibrated via MD runs in the isothermal-isobaric (NPT) ensemble, with a time step of 1 fs. All restraints on the protein atoms were then removed, and each system was further equilibrated using NPT MD runs at 298vK. Three equilibration steps were performed (4 ns each, time step 2.0 fs). System stability was monitored by the fluctuations of the root-mean-square-deviation (rmsd) of the simulated position of the backbone atoms of the protein with respect to those of the initial protein model. The equilibration phase was followed by a data production run consisting of 50 ns of MD simulations in the NVT ensemble. Data collection was performed on over the last 20 ns of each equilibrated MD trajectory were considered for statistical data collections. 1000 trajectory snapshots were analyzed for each **18**/receptor complex. The free energy of binding ΔG_{bind} between **18** and the target proteins was estimated by resorting to the well-validated Molecular Mechanics/Poisson-Boltzmann Surface Area (MM/PBSA) approach [71] implemented in Amber 16. The per residue binding free energy decomposition (interaction spectra) was carried out using the Molecular Mechanics/Generalized Boltzmann Surface Area (MM/GBSA) approach [93,94], and was based on the same snapshots used in the binding free energy calculation.

Acknowledgments

Financial supports from the Spanish Ministry of Economy, Industry, and Competitiveness (MEICOM, grant SAF2015-64948-C2-1-R to MIRF; grant SAF2014-52940-R to APC), Consejo Superior de Investigaciones Científicas (CSIC, grant PIE-201580E109 to MIRF), and Dirección General de Investigación e Innovación de la Comunidad de Madrid (DGII-CM, grant B2017/BMD-3827, acronym NRF24AD-CM to MIRF) are gratefully acknowledged. DV thanks financial support from the Consellería de Cultura, Educación e Ordenación Universitaria and Centro Singular de Investigación de Galicia (accreditation 2016-2019, ED431G/05) and the European Regional Development Fund (ERDF). MEV thanks COLCIENCIAS (Colombia) for a Ph.D. fellowship.

Appendix A. Supplementary data

Supplementary data associated with this article can be found in the online version. These data include synthesis of intermediates, kinetic studies in human AChE and *in silico* medicinal chemistry alerts of DFHs **1-29**.

REFERENCES

- [1] P. Maresova, H. Mohelska, J. Dolejs, K. Kuca, Socio-economic Aspects of Alzheimer's Disease, *Curr. Alzheimer Res.* 12 (2015) 903-911.
- [2] P. Scheltens, K. Blennow, M.M. Breteler, B. de Strooper, G.B. Frisoni, S. Salloway, W.M. Van der Flier, Alzheimer's disease, *Lancet* 388 (2016) 505-517.
- [3] C.C. Tan, J.T. Yu, H.F. Wang, M.S. Tan, X.F. Meng, C. Wang, T. Jiang, X.C. Zhu, L. Tan, Efficacy and safety of donepezil, galantamine, rivastigmine, and memantine for the treatment of Alzheimer's disease: a systematic review and meta-analysis, *J. Alzheimer's Dis.* 41 (2014) 615-631.
- [4] A. Atri, S.B. Hendrix, V. Pejovic, R.K. Hofbauer, J. Edwards, J.L. Molinuevo, S.M. Graham, Cumulative, additive benefits of memantine-donepezil combination over component monotherapies in moderate to severe Alzheimer's dementia: a pooled area under the curve analysis, *Alzheimers Res. Ther.* 7 (2015) 28.
- [5] R. Morphy, Z. Rankovic, Designed multiple ligands. An emerging drug discovery paradigm, *J. Med. Chem.* 48 (2005) 6523-6543.
- [6] D. Panek, A. Wieckowska, T. Wichur, M. Bajda, J. Godyn, J. Jonczyk, K. Mika, J. Janockova, O. Soukup, D. Knez, J. Korabecny, S. Gobec, B. Malawska, Design, synthesis and biological evaluation of new phthalimide and saccharin derivatives with alicyclic amines targeting cholinesterases, beta-secretase and amyloid beta aggregation, *Eur. J. Med. Chem.* 125 (2017) 676-695.
- [7] R.H. Swerdlow, Alzheimer's disease pathologic cascades: who comes first, what drives what, *Neurotox. Res.* 22 (2012) 182-194.
- [8] J. Hroudova, N. Singh, Z. Fisar, K.K. Ghosh, Progress in drug development for Alzheimer's disease: An overview in relation to mitochondrial energy metabolism, *Eur. J. Med. Chem.* 121 (2016) 774-784.

- [9] M.A. Ansari, S.W. Scheff, Oxidative stress in the progression of Alzheimer disease in the frontal cortex, *J. Neuropathol. Exp. Neurol.* 69 (2010) 155-167.
- [10] A.E. Moneim, Oxidant/Antioxidant imbalance and the risk of Alzheimer's disease, *Curr. Alzheimer Res.* 12 (2015) 335-349.
- [11] C. Fernández-Moriano, E. González-Burgos, M.P. Gómez-Serranillos, Mitochondria-Targeted Protective Compounds in Parkinson's and Alzheimer's Diseases, *Oxid. Med. Cell. Longev.* 2015 (2015) 408927.
- [12] B.P. Imbimbo, V. Solfrizzi, F. Panza, Are NSAIDs useful to treat Alzheimer's disease or mild cognitive impairment?, *Front. Aging Neurosci.* 2 (2010).
- [13] M.D. Ikonovic, E.E. Abrahamson, T. Uz, H. Manev, S.T. Dekosky, Increased 5-lipoxygenase immunoreactivity in the hippocampus of patients with Alzheimer's disease, *J. Histochem. Cytochem.* 56 (2008) 1065-1073.
- [14] J. Chu, P.F. Giannopoulos, C. Ceballos-Díaz, T.E. Golde, D. Praticò, 5-Lipoxygenase gene transfer worsens memory, amyloid, and tau brain pathologies in a mouse model of Alzheimer disease, *Ann. Neurol.* 72 (2012) 442-454.
- [15] K.J. Herbst-Robinson, L. Liu, M. James, Y. Yao, S.X. Xie, K.R. Brunden, Inflammatory Eicosanoids Increase Amyloid Precursor Protein Expression via Activation of Multiple Neuronal Receptors, *Sci. Rep.* 5 (2015) 18286.
- [16] D. Steinhilber, B. Hofmann, Recent advances in the search for novel 5-lipoxygenase inhibitors, *Basic Clin. Pharmacol. Toxicol.* 114 (2014) 70-77.
- [17] Z. Cai, Monoamine oxidase inhibitors: promising therapeutic agents for Alzheimer's disease (Review), *Mol. Med. Rep.* 9 (2014) 1533-1541.
- [18] S. Schedin-Weiss, M. Inoue, L. Hromadkova, Y. Teranishi, N.G. Yamamoto, B. Wiehager, N. Bogdanovic, B. Winblad, A. Sandebring-Matton, S. Frykman, L.O. Tjernberg, Monoamine oxidase B is elevated in Alzheimer disease neurons, is

associated with gamma-secretase and regulates neuronal amyloid beta-peptide levels, *Alzheimers Res. Ther.* 9 (2017) 57.

[19] D. Knez, M. Sova, U. Kosak, S. Gobec, Dual inhibitors of cholinesterases and monoamine oxidases for Alzheimer's disease, *Future Med. Chem.* 9 (2017) 811-832.

[20] M. Yáñez, D. Viña, Dual inhibitors of monoamine oxidase and cholinesterase for the treatment of Alzheimer disease, *Curr. Top. Med. Chem.* 13 (2013) 1692-1706.

[21] K.L. Jansen, R.L. Faull, M. Dragunow, R.A. Leslie, Autoradiographic distribution of sigma receptors in human neocortex, hippocampus, basal ganglia, cerebellum, pineal and pituitary glands, *Brain Res.* 559 (1991) 172-177.

[22] A. Pal, D. Fontanilla, A. Gopalakrishnan, Y.K. Chae, J.L. Markley, A.E. Ruoho, The sigma-1 receptor protects against cellular oxidative stress and activates antioxidant response elements, *Eur. J. Pharmacol.* 682 (2012) 12-20.

[23] A. Klouz, D.B. Said, H. Ferchichi, N. Kourda, L. Ouanes, M. Lakhal, J.P. Tillement, D. Morin, Protection of cellular and mitochondrial functions against liver ischemia by N-benzyl-N'-(2-hydroxy-3,4-dimethoxybenzyl)-piperazine (BHDP), a sigma1 ligand, *Eur. J. Pharmacol.* 578 (2008) 292-299.

[24] Clinical trials database: NCT02244541.
<https://www.clinicaltrials.gov/ct2/show/NCT02244541>.

[25] C. Rolando, V. Taylor, Neural stem cell of the hippocampus: development, physiology regulation, and dysfunction in disease, *Curr. Top. Dev. Biol.* 107 (2014) 183-206.

[26] G. Kempermann, S. Jessberger, B. Steiner, G. Kronenberg, Milestones of neuronal development in the adult hippocampus, *Trends Neurosci.* 27 (2004) 447-452.

- [27] C. Herrera-Arozamena, O. Martí-Marí, M. Estrada, M. de la Fuente Revenga, M.I. Rodríguez-Franco, Recent advances in neurogenic small molecules as innovative treatments for neurodegenerative diseases, *Molecules* 21 (2016) 1165-1185.
- [28] P. Ambrogini, M. Betti, C. Galati, M. Di Palma, D. Lattanzi, D. Savelli, F. Galli, R. Cuppini, A. Minelli, alpha-Tocopherol and Hippocampal Neural Plasticity in Physiological and Pathological Conditions, *Int. J. Mol. Sci.* 17 (2016).
- [29] S. Moriguchi, Y. Shinoda, Y. Yamamoto, Y. Sasaki, K. Miyajima, H. Tagashira, K. Fukunaga, Stimulation of the sigma-1 receptor by DHEA enhances synaptic efficacy and neurogenesis in the hippocampal dentate gyrus of olfactory bulbectomized mice, *PLoS One* 8 (2013) e60863.
- [30] I. Kusumi, S. Boku, Y. Takahashi, Psychopharmacology of atypical antipsychotic drugs: From the receptor binding profile to neuroprotection and neurogenesis, *Psychiatry Clin. Neurosci.* 69 (2015) 243-258.
- [31] G.C. González-Muñoz, M.P. Arce, C. Pérez, A. Romero, M. Villarroya, M.G. López, S. Conde, M.I. Rodríguez-Franco, Dibenzo[1,4,5]thiadiazepine: a hardly-known heterocyclic system with neuroprotective properties of potential usefulness in the treatment of neurodegenerative diseases, *Eur. J. Med. Chem.* 81 (2014) 350-358.
- [32] L. Monjas, M.P. Arce, R. León, J. Egea, C. Pérez, M. Villarroya, M.G. López, C. Gil, S. Conde, M.I. Rodríguez-Franco, Enzymatic and solid-phase synthesis of new donepezil-based L- and D-glutamic acid derivatives and their pharmacological evaluation in models related to Alzheimer's disease and cerebral ischemia, *Eur. J. Med. Chem.* 130 (2017) 60-72.
- [33] M. de la Fuente Revenga, C. Pérez, J.A. Morales-García, S. Alonso-Gil, A. Pérez-Castillo, D.H. Caignard, M. Yáñez, A.M. Gamo, M.I. Rodríguez-Franco, Neurogenic Potential Assessment and Pharmacological Characterization of 6-Methoxy-1,2,3,4-

tetrahydro-beta-carboline (Pinoline) and Melatonin-Pinoline Hybrids, ACS Chem. Neurosci 6 (2015) 800-810.

[34] M. de la Fuente Revenga, N. Fernández-Sáez, C. Herrera-Arozamena, J.A. Morales-García, S. Alonso-Gil, A. Pérez-Castillo, D.H. Caignard, S. Rivara, M.I. Rodríguez-Franco, Novel *N*-Acetyl Bioisosteres of Melatonin: Melatonergic Receptor Pharmacology, Physicochemical Studies, and Phenotypic Assessment of Their Neurogenic Potential, J. Med. Chem. 58 (2015) 4998-5014.

[35] M. Estrada, C. Pérez, E. Soriano, E. Laurini, M. Romano, S. Pricl, J.A. Morales-García, A. Pérez-Castillo, M.I. Rodríguez-Franco, New neurogenic lipoic-based hybrids as innovative Alzheimer's drugs with sigma-1 agonism and beta-secretase inhibition, Future Med. Chem. 8 (2016) 1191-1207.

[36] J.A. Morales-García, M. de la Fuente Revenga, S. Alonso-Gil, M.I. Rodríguez-Franco, A. Feilding, A. Perez-Castillo, J. Riba, The alkaloids of *Banisteriopsis caapi*, the plant source of the Amazonian hallucinogen Ayahuasca, stimulate adult neurogenesis *in vitro*, Sci. Rep. 7 (2017) 5309.

[37] B. López-Iglesias, C. Pérez, J.A. Morales-García, S. Alonso-Gil, A. Pérez-Castillo, A. Romero, M.G. López, M. Villarroja, S. Conde, M.I. Rodríguez-Franco, New melatonin-*N,N*-dibenzyl(*N*-methyl)amine hybrids: potent neurogenic agents with antioxidant, cholinergic, and neuroprotective properties as innovative drugs for Alzheimer's disease, J. Med. Chem. 57 (2014) 3773-3785.

[38] M. Estrada, C. Herrera-Arozamena, C. Pérez, D. Viña, A. Romero, J.A. Morales-García, A. Pérez-Castillo, M.I. Rodríguez-Franco, New cinnamic - *N*-benzylpiperidine and cinnamic - *N,N*-dibenzyl(*N*-methyl)amine hybrids as Alzheimer-directed multitarget drugs with antioxidant, cholinergic, neuroprotective and neurogenic properties, Eur. J. Med. Chem. 121 (2016) 376-386.

- [39] J. Meunier, J. Ieni, T. Maurice, The anti-amnesic and neuroprotective effects of donepezil against amyloid beta₂₅₋₃₅ peptide-induced toxicity in mice involve an interaction with the sigma₁ receptor, *Br. J. Pharmacol.* 149 (2006) 998-1012.
- [40] S. Carradori, M.C. Gidaro, A. Petzer, G. Costa, P. Guglielmi, P. Chimenti, S. Alcaro, J.P. Petzer, Inhibition of Human Monoamine Oxidase: Biological and Molecular Modeling Studies on Selected Natural Flavonoids, *J. Agric. Food Chem.* 64 (2016) 9004-9011.
- [41] D. Ribeiro, M. Freitas, S.M. Tome, A.M. Silva, G. Porto, E.J. Cabrita, M.M. Marques, E. Fernandes, Inhibition of LOX by flavonoids: a structure-activity relationship study, *Eur. J. Med. Chem.* 72 (2014) 137-145.
- [42] C. Pergola, O. Werz, 5-Lipoxygenase inhibitors: a review of recent developments and patents, *Expert Opin. Ther. Pat.* 20 (2010) 355-375.
- [43] R.J. Williams, J.P. Spencer, Flavonoids, cognition, and dementia: actions, mechanisms, and potential therapeutic utility for Alzheimer disease, *Free Radic. Biol. Med.* 52 (2012) 35-45.
- [44] Y. Lee, S.J. Jeon, H.E. Lee, I.H. Jung, Y.W. Jo, S. Lee, J.H. Cheong, D.S. Jang, J.H. Ryu, Spinosin, a C-glycoside flavonoid, enhances cognitive performance and adult hippocampal neurogenesis in mice, *Pharmacol. Biochem. Behav.* 145 (2016) 9-16.
- [45] Z. Fu, X. Li, Y. Miao, K.M. Merz, Jr., Conformational analysis and parallel QM/MM X-ray refinement of protein bound anti-Alzheimer drug donepezil, *J. Chem. Theory Comput.* 9 (2013) 1686-1693.
- [46] M.I. Fernández-Bachiller, C. Pérez, L. Monjas, J. Rademann, M.I. Rodríguez-Franco, New tacrine – 4-oxo-4*H*-chromene hybrids as multifunctional agents for the treatment of Alzheimer's disease, with cholinergic, antioxidant, and beta-amyloid-reducing properties, *J. Med. Chem.* 55 (2012) 1303-1317.

- [47] G.A. Czapski, K. Czubowicz, R.P. Strosznajder, Evaluation of the antioxidative properties of lipoxygenase inhibitors, *Pharmacol. Rep.* 64 (2012) 1179-1188.
- [48] O. Mazzoni, G. Esposito, M.V. Diurno, D. Brancaccio, A. Carotenuto, P. Grieco, E. Novellino, W. Filippelli, Synthesis and pharmacological evaluation of some 4-oxo-quinoline-2-carboxylic acid derivatives as anti-inflammatory and analgesic agents, *Arch. Pharm.* 343 (2010) 561-569.
- [49] J.F.W. McOmie, M.L. Watts, D.E. West, Demethylation of aryl methyl ethers by boron tribromide, *Tetrahedron* 24 (1968) 2289-2292.
- [50] G.L. Ellman, K.D. Courtney, V. Andres, Jr., R.M. Feather-Stone, A new and rapid colorimetric determination of acetylcholinesterase activity, *Biochem. Pharmacol.* 7 (1961) 88-95.
- [51] L. Di, E.H. Kerns, K. Fan, O.J. McConnell, G.T. Carter, High throughput artificial membrane permeability assay for blood-brain barrier, *Eur. J. Med. Chem.* 38 (2003) 223-232.
- [52] M.I. Rodríguez-Franco, M.I. Fernández-Bachiller, C. Pérez, B. Hernández-Ledesma, B. Bartolomé, Novel tacrine-melatonin hybrids as dual-acting drugs for Alzheimer disease, with improved acetylcholinesterase inhibitory and antioxidant properties, *J. Med. Chem.* 49 (2006) 459-462.
- [53] M.I. Fernández-Bachiller, C. Pérez, L. Monjas, J. Rademann, M.I. Rodríguez-Franco, New tacrine-4-oxo-4*H*-chromene hybrids as multifunctional agents for the treatment of Alzheimer's disease, with cholinergic, antioxidant, and beta-amyloid-reducing properties, *J. Med. Chem.* 55 (2012) 1303-1317.
- [54] M. de la Fuente Revenga, N. Fernández-Sáez, C. Herrera-Arozamena, J.A. Morales-García, S. Alonso-Gil, A. Pérez-Castillo, D.H. Caignard, S. Rivara, M.I. Rodríguez-Franco, Novel *N*-acetyl bioisosteres of melatonin: melatonergic receptor

pharmacology, physicochemical studies, and phenotypic assessment of their neurogenic potential, *J. Med. Chem.* 58 (2015) 4998-5014.

[55] R.A. Pufahl, T.P. Kasten, R. Hills, J.K. Gierse, B.A. Reitz, R.A. Weinberg, J.L. Masferrer, Development of a fluorescence-based enzyme assay of human 5-lipoxygenase, *Anal. Biochem.* 364 (2007) 204-212.

[56] J.P. Finberg, J.M. Rabey, Inhibitors of MAO-A and MAO-B in Psychiatry and Neurology, *Front. Pharmacol.* 7 (2016) 340.

[57] U.B. Chu, A.E. Ruoho, Sigma Receptor Binding Assays, *Curr. Protoc. Pharmacol.* 71 (2015) 1 34 31-21.

[58] T. Sterling, J.J. Irwin, ZINC 15--Ligand Discovery for Everyone, *J. Chem. Inf. Model.* 55 (2015) 2324-2337.

[59] A. Daina, O. Michielin, V. Zoete, SwissADME: a free web tool to evaluate pharmacokinetics, drug-likeness and medicinal chemistry friendliness of small molecules, *Sci. Rep.* 7 (2017) 42717.

[60] R. Brenk, A. Schipani, D. James, A. Krasowski, I.H. Gilbert, J. Frearson, P.G. Wyatt, Lessons learnt from assembling screening libraries for drug discovery for neglected diseases, *ChemMedChem* 3 (2008) 435-444.

[61] A. Romero, J. Egea, G.C. González-Muñoz, M.D. Martín de Saavedra, L. del Barrio, M.I. Rodríguez-Franco, S. Conde, M.G. López, M. Villarroya, C. de los Ríos, ITH12410/SC058: a new neuroprotective compound with potential in the treatment of Alzheimer's disease, *ACS Chem. Neurosci.* 5 (2014) 770-775.

[62] N. Li, K. Ragheb, G. Lawler, J. Sturgis, B. Rajwa, J.A. Melendez, J.P. Robinson, Mitochondrial complex I inhibitor rotenone induces apoptosis through enhancing mitochondrial reactive oxygen species production, *J. Biol. Chem.* 278 (2003) 8516-8525.

- [63] R.J. Devenish, M. Prescott, G.M. Boyle, P. Nagley, The oligomycin axis of mitochondrial ATP synthase: OSCP and the proton channel, *J. Bioenerg. Biomembr.* 32 (2000) 507-515.
- [64] P.W. Sylvester, Optimization of the tetrazolium dye (MTT) colorimetric assay for cellular growth and viability, *Methods Mol. Biol.* 716 (2011) 157-168.
- [65] J.A. Morales-García, S. Alonso-Gil, C. Gil, A. Martínez, A. Santos, A. Pérez-Castillo, Phosphodiesterase 7 inhibition induces dopaminergic neurogenesis in hemiparkinsonian rats, *Stem Cells Transl. Med.* 4 (2015) 564-575.
- [66] J.A. Morales-García, R. Luna-Medina, C. Alfaro-Cervello, M. Cortés-Canteli, A. Santos, J.M. García-Verdugo, A. Pérez-Castillo, Peroxisome proliferator-activated receptor gamma ligands regulate neural stem cell proliferation and differentiation *in vitro* and *in vivo*, *Glia* 59 (2011) 293-307.
- [67] J.A. Morales-García, R. Luna-Medina, S. Alonso-Gil, M. Sanz-Sancristóbal, V. Palomo, C. Gil, A. Santos, A. Martínez, A. Pérez-Castillo, Glycogen synthase kinase 3 inhibition promotes adult hippocampal neurogenesis *in vitro* and *in vivo*, *ACS Chem. Neurosci.* 3 (2012) 963-971.
- [68] C.A. Marchant, K.A. Briggs, A. Long, *In silico* tools for sharing data and knowledge on toxicity and metabolism: Derek for windows, meteor, and vitic, *Toxicol. Mech. Methods* 18 (2008) 177-187.
- [69] P.N. Judson, S.A. Stalford, J. Vessey, Assessing confidence in predictions made by knowledge-based systems, *Toxicol. Res.* 2 (2013) 70-79.
- [70] G.M. Morris, R. Huey, W. Lindstrom, M.F. Sanner, R.K. Belew, D.S. Goodsell, A.J. Olson, AutoDock4 and AutoDockTools4: Automated docking with selective receptor flexibility, *J. Comput. Chem.* 30 (2009) 2785-2791.

- [71] I. Massova, P.A. Kollman, Combined molecular mechanical and continuum solvent approach (MM-PBSA/GBSA) to predict ligand binding, *Perspect. Drug Discov.* 18 (2000) 113-135.
- [72] J. Cheung, M.J. Rudolph, F. Burshteyn, M.S. Cassidy, E.N. Gary, J. Love, M.C. Franklin, J.J. Height, Structures of human acetylcholinesterase in complex with pharmacologically important ligands, *J. Med. Chem.* 55 (2012) 10282-10286.
- [73] M. Hadjeri, M. Barbier, X. Ronot, A.M. Mariotte, A. Boumendjel, J. Boutonnat, Modulation of P-glycoprotein-mediated multidrug resistance by flavonoid derivatives and analogues, *J. Med. Chem.* 46 (2003) 2125-2131.
- [74] J. Reis, A. Gaspar, F. Borges, L. Rebelo Gomes, J.N. Low, Synthesis, spectroscopic characterization and X-ray structure of novel 7-methoxy-4-oxo-N-phenyl-4*H*-chromene-2-carboxamides, *J. Molec. Struct.* 1056–1057 (2014) 31-37.
- [75] G. Mouysset, M. Payard, P. Tronche, J. Bastide, P. Bastide, Synthesis and antiallergic activity of some benzopyronic and structurally related alcohols, *Eur. J. Med. Chem.* 23 (1988) 199-202.
- [76] D. Zewge, C.Y. Chen, C. Deer, P.G. Dormer, D.L. Hughes, A mild and efficient synthesis of 4-quinolones and quinolone heterocycles, *J. Org. Chem.* 72 (2007) 4276-4279.
- [77] D. Edmont, R. Rocher, C. Plisson, J. Chenault, Synthesis and evaluation of quinoline carboxyguanidines as antidiabetic agents, *Bioorg. Med. Chem. Lett.* 10 (2000) 1831-1834.
- [78] M. Albrecht, O. Osetska, T. Rantanen, R. Froehlich, C. Bolm, Microwave-assisted preparation of quinolone and quinoline derivatives, *Synlett* (2010) 1081-1084.
- [79] J. Bryant, B. Buckman, I. Islam, R. Mohan, M. Morrissey, G.P. Wei, W. Xu, S. Yuan, A preparation of 2-aminocarbonylquinoline derivatives, useful as platelet

adenosine diphosphate receptor antagonists, PCT Int. Appl. WO 2004052366 A1 20040624 (2004).

[80] M.J. Matos, F. Rodríguez-Enríquez, F. Borges, L. Santana, E. Uriarte, M. Estrada, M.I. Rodríguez-Franco, R. Laguna, D. Viña, 3-Amidocoumarins as Potential Multifunctional Agents against Neurodegenerative Diseases, *ChemMedChem* 10 (2015) 2071-2079.

[81] A. Dávalos, C. Gómez-Cordovés, B. Bartolomé, Extending applicability of the oxygen radical absorbance capacity (ORAC-fluorescein) assay, *J. Agric. Food Chem.* 52 (2004) 48-54.

[82] F. Denizot, R. Lang, Rapid colorimetric assay for cell growth and survival. Modifications to the tetrazolium dye procedure giving improved sensitivity and reliability, *J. Immunol. Methods* 89 (1986) 271-277.

[83] D.A. Case, R.M. Betz, W. Botello-Smith, D.S. Cerutti, T.E.I. Cheatham, T.A. Darden, R.E. Duke, T.J. Giese, H. Gohlke, A.W. Goetz, N. Homeyer, S. Izadi, P. Janowski, J. Kaus, A. Kovalenko, T.S. Lee, S. LeGrand, P. Li, C. Lin, T. Luchko, R. Luo, B. Madej, D. Mermelstein, K.M. Merz, G. Monard, H. Nguyen, H.T. Nguyen, I. Omelyan, A. Onufriev, D.R. Roe, A. Roitberg, C. Sagui, C.L. Simmerling, J. Swails, R.C. Walker, J. Wang, R.M. Wolf, X. Wu, L. Xiao, D.M. York, P.A. Kollman, AMBER, University of California, San Francisco (CA, USA), **2016**.

[84] E.F. Pettersen, T.D. Goddard, C.C. Huang, G.S. Couch, D.M. Greenblatt, E.C. Meng, T.E. Ferrin, UCSF Chimera--a visualization system for exploratory research and analysis, *J. Comput. Chem.* 25 (2004) 1605-1612.

[85] N.C. Gilbert, Z. Rui, D.B. Neau, M.T. Waight, S.G. Bartlett, W.E. Boeglin, A.R. Brash, M.E. Newcomer, Conversion of human 5-lipoxygenase to a 15-lipoxygenase by

a point mutation to mimic phosphorylation at Serine-663, *FASEB J.* 26 (2012) 3222-3229.

[86] H.R. Schmidt, S. Zheng, E. Gurpinar, A. Koehl, A. Manglik, A.C. Kruse, Crystal structure of the human σ_1 receptor, *Nature* 532 (2016) 527.

[87] E. Laurini, V.D. Col, M.G. Mamolo, D. Zampieri, P. Posocco, M. Fermeglia, L. Vio, S. Pricl, Homology Model and Docking-Based Virtual Screening for Ligands of the sigma1 Receptor, *ACS Med. Chem. Lett.* 2 (2011) 834-839.

[88] S. Brune, D. Schepmann, K.H. Klempnauer, D. Marson, V. Dal Col, E. Laurini, M. Fermeglia, B. Wunsch, S. Pricl, The sigma enigma: in vitro/in silico site-directed mutagenesis studies unveil sigma1 receptor ligand binding, *Biochemistry* 53 (2014) 2993-3003.

[89] E. Laurini, D. Marson, V. Dal Col, M. Fermeglia, M.G. Mamolo, D. Zampieri, L. Vio, S. Pricl, Another Brick in the Wall. Validation of the σ_1 Receptor 3D Model by Computer-Assisted Design, Synthesis, and Activity of New σ_1 Ligands, *Mol. Pharm.* 9 (2012) 3107-3126.

[90] E. Laurini, V. Da Col, B. Wunsch, S. Pricl, Analysis of the molecular interactions of the potent analgesic S1RA with the sigma1 receptor, *Bioorg. Med. Chem. Lett.* 23 (2013) 2868-2871.

[91] I. Briguglio, R. Loddo, E. Laurini, M. Fermeglia, S. Piras, P. Corona, P. Giunchedi, E. Gavini, G. Sanna, G. Giliberti, C. Ibba, P. Farci, P. La Colla, S. Pricl, A. Carta, Synthesis, cytotoxicity and antiviral evaluation of new series of imidazo[4,5-g]quinoline and pyrido[2,3-g]quinoxalinone derivatives, *Eur. J. Med. Chem.* 105 (2015) 63-79.

[92] W.L. Jorgensen, J. Chandrasekhar, J.D. Madura, R.W. Impey, M.L. Klein, Comparison of simple potential functions for simulating liquid water, *J. Chem. Phys.* 79 (1983) 926-935.

[93] V. Tsui, D.A. Case, Theory and applications of the generalized Born solvation model in macromolecular simulations, *Biopolymers* 56 (2000) 275-291.

[94] A. Onufriev, D. Bashford, D.A. Case, Modification of the generalized Born model suitable for macromolecules, *J. Phys. Chem. B* 104 (2000) 3712-3720.

ACCEPTED MANUSCRIPT